Title: Collaborative Cross strains reveal that *Irf3* deficiency results in uncontrolled Zika virus replication *in vitro* but is insufficient to induce disease susceptibility in mice.

Running title: *Irf3* deficiency promotes ZIKV replication

Marie Bourdon[§1], Caroline Manet[§1], Laurine Conquet[1], Corentin Ramaugé-Parra[1], Etienne Kornobis[2], Eliette Bonnefoy[3], Xavier Montagutelli[#1]

[1]Institut Pasteur, Université de Paris, Mouse Genetics Laboratory, F-75015 Paris, France

[2]Institut Pasteur, Université de Paris, Biomics, F-75015 Paris, France

[3]Université Paris Cité, Institut Cochin, Inserm, CNRS, F-75014 Paris, France

[§] M.B. and C. M. equally contributed to this work and are co-first authors

[#] Corresponding author: xavier.montagutelli@pasteur.fr

Keywords: Zika virus, mouse, Irf3, interferon response, Collaborative Cross, susceptibility

Abstract

Zika virus (ZIKV) is a Flavivirus responsible for recent epidemics in Pacific Islands and in the Americas. In humans, the consequences of ZIKV infection range from asymptomatic infection to severe neurological disease such as Guillain-Barré syndrome or fetal neurodevelopmental defects, suggesting the influence of host genetic factors. We previously reported similar diverse outcomes of ZIKV infection in mice of the Collaborative Cross, a collection of inbred strains with large genetic diversity. CC071 was the most susceptible strain with severe symptoms and lethality. Here, we investigated viral replication in mouse embryonic fibroblasts from CC071 and two resistant strains. CC071 showed enhanced viral replication associated with delayed induction of type-I interferons (IFN-I). Using a combination of genetic approaches, we identified a loss of function (LOF) mutation in the *Irf3* gene, specific to CC071, and demonstrated that it fully explains the defective IFN-I response and uncontrolled viral replication in CC071 MEFs. However, this mutation was not sufficient to induce the high plasma viral load and clinical severity observed in CC071 mice, indicating the involvement of other susceptibility genes *in vivo*. Considering the susceptibility of the CC071 strain to multiple viruses, our results provide new insight into the role of *Irf3* in innate antiviral response.

Importance

Recent ZIKV outbreaks led to millions of infected people, with rare but severe complications such as Guillain-Barré syndrome and encephalitis in adults suggesting host genetic control. We previously reported the importance of host genes in ZIKV pathogenesis using a panel of genetically diverse mouse strains and identified CC071 as the most susceptible strain. Through a combination of functional and genetic approaches in a cellular model, we identified a mutation in the *Irf3* gene which plays a key role in the expression of interferon beta. This mutation fully explains the high viral replication observed in CC071 cells. However, it was not sufficient to explain the symptoms displayed by CC071 ZIKV-infected mice, unraveling the implication of other host genes. Since CC071 has been reported as a valuable model for several viral infections, our results have implications beyond ZIKV infection and contribute to shedding light on host mechanisms fighting infectious diseases.

Introduction

Zika virus (ZIKV) is a mosquito-borne virus of the *Flaviviridae* family identified in 1947 in Uganda. The first noticeable human outbreaks occurred in Micronesia in 2007 and in French Polynesia and New Caledonia in 2013-2014. In 2015-2016, ZIKV caused an epidemic in Brazil which rapidly spread across the Americas and the Caribbean. To date, 89 countries have reported evidence of mosquito-transmitted Zika virus infection (https://www.who.int/health-topics/zika-virus-disease#tab=tab_1).

While most people infected with ZIKV remain asymptomatic, some develop non-specific symptoms including rash, fever, conjunctivitis, muscle and joint pain, malaise and headache. Neurological complications have been described in adults such as Guillain-Barré syndrome (1) and encephalitis (2). Infection of pregnant women was associated with congenital Zika syndrome in the fetus, which can lead to neurodevelopmental deficiencies, brain malformation (3) or in some cases to fetal loss (4).

Many factors may contribute to this variable severity, including the viral strain, the infection route and dose, and the host genetic background (5, 6). Indeed, mouse and human studies have shown that host genes influence flaviviral infections' outcomes (7). While human genetic studies are hampered by the variability of these multiple factors, they can be controlled in mouse models which have proven very valuable to identify susceptibility variants (8, 9). Relevant ZIKV infection models have been developed in mice either using *Ifnar1* knock-out (KO) mice in which the IFNAR receptor to IFN-I has been inactivated (10, 11), or by blocking this receptor using a monoclonal antibody targeting the IFNAR1 receptor subunit (MAR1-5A3 (12)).

We have previously explored the role of mouse natural genetic variants on ZIKV susceptibility in the Collaborative Cross (CC), a panel of recombinant inbred mice encompassing a genetic diversity similar to that of the human population and capturing approximately 90% of the mouse natural genetic variants (13, 14). We reported that the CC genetic diversity enabled large variations in the clinical severity of ZIKV disease, plasma viral load and intensity of brain pathology (15). We specifically identified CC071 mice as very susceptible, with high mortality and high peak plasma viral load. We also demonstrated that genetic background influenced the control of ZIKV replication in CC mouse embryonic fibroblasts (MEFs).

Here, we investigated the mechanisms driving high viral replication in CC071 MEFs. We found that, compared with the more resistant C57BL/6J (B6) and CC001 strains, ZIKV-infected CC071

MEFs displayed a delayed expression of the IFN-I response genes. Genetic and functional analyses identified a strain-specific, LOF variant in the *Irf3* gene, the main transcription factor involved in IFN-I expression. *In vivo* comparison of CC071 and B6-*Irf3* KO mice showed that *Irf3* deficit is not sufficient to explain the high susceptibility of CC071 mice to ZIKV infection, unraveling the plurality of genetic factors controlling susceptibility to viral infections. These findings provide new insights on the role of *Irf3* in viral diseases and exemplify how the study of CC strains allows deciphering the role of host genes in ZIKV and other viruses' pathogenesis.

Results

CC071 MEFs show defective control of viral replication and delayed IFN-I expression, but normal response to IFN-I stimulation

We previously reported that, unlike CC001 MEFs, CC071 MEFs produced increasing quantities of viral particles during the first 72 hours post-infection (hpi) (15). Here, we confirmed and expanded this observation by infecting B6, CC001 and CC071 MEFs and by quantifying viral particles by FFA. After ZIKV infection, CC071 MEFs displayed high and increasing viral titers between 24 and 72 hpi, while CC001 and B6 MEFs showed stable and lower titers (Fig 1A).

To investigate the origin of the defective control of viral replication in CC071 MEFs, we measured the expression level of the *Ifnb1* gene coding for IFNβ in ZIKV-infected CC071, CC001 and B6 MEFs. *Ifnb1* expression is induced very rapidly after virus detection by sensors and triggers the innate antiviral response which is essential for limiting viral replication. In CC001 and B6 MEFs, *Ifnb1* expression was significantly induced at 24 hpi and remained stable and high until at least 72 hpi (Fig 1B). In contrast, its expression in CC071 MEFs was low at 24 hpi and reached the level of CC001 only at 72 hpi. Similar results were obtained for *Ifn4a* which encodes one of the IFNα proteins (Sup Fig 1). Notably, *Ifnb1* expression in CC071 MEFs at 72 hpi was significantly higher than in B6 MEFs, showing that CC071 MEFs were delayed but not intrinsically hampered in their ability to induce a strong IFN-I expression.

To test whether this defective induction of *Ifnb1* expression was specific to ZIKV infection, MEFs were then transfected with the influenza A virus-derived 3-phosphate-hairpin-RNA (3p-hpRNA), an agonist of the RIG-I/MDA5-MAVS pathway, or treated with polyinosine-polycytidylic acid (poly (I:C)), that stimulates both Toll-like receptor 3 (TLR3) and the RIG-I/MDA5-MAVS pathway (16). Here again, CC071 MEFs showed a delayed expression of *Ifnb1* by comparison with B6 and CC001 MEFs (Sup Fig 2), indicating that the defect in IFN-I genes expression in CC071 MEFs was not specific to ZIKV infection. This result suggested a defect in the molecular cascade between cellular sensors of pathogen-associated molecular patterns (PAMP) and the *Ifnb1* gene transcription machinery.

To evaluate the capacity of CC071 MEFs to respond to IFN-I stimulation, they were treated with recombinant IFNα. The expression of IFN-stimulated genes (ISGs) such as *Ifitm3* was induced with the same kinetics and level as in B6 and CC001 MEFs (Fig 1C), showing that CC071

120 MEFs are able to respond normally to IFN-I stimulation and that their defect is limited to the
121 induction of *Ifnb1* gene expression.
122
123 *CC071's delayed Ifnb1 expression is strain-specific*
124 To gain insight into the mechanisms responsible for defective *Ifnb1* induction, we investigated
125 the expression levels of all genes involved in *Ifnb1* expression on CC071, B6 and CC001 MEFs
126 at 16, 24 and 32 hpi. Mock-infected MEFs were analyzed at 24 hours as controls. Expression
127 levels were measured by RNA sequencing (RNAseq) which provided a comprehensive analysis
128 of transcriptomic changes. In CC001 MEFs, the expression of many genes rapidly increased
129 after infection (160 at 16h, 821 at 24h and 971 at 32h; log2 fold-change > 1, FDR = 0.05),
130 reflecting a robust innate antiviral response (Sup Fig 3A). A similar pattern was observed in B6
131 MEFs. By contrast, the expression of only 38 genes was increased in CC071 MEFs at 32hpi (34
132 of which were also activated in CC001), consistent with the delayed induction of *Ifnb1*
133 expression. Among the genes that are involved in the pathway between PAMP sensors and
134 *Ifnb1* transcription, ISGs such as *Tlr3*, *Ddx58* (coding for RIG-I sensor) or *Irf7* were not activated
135 upon infection in CC071, while constitutively expressed genes such as *Mavs*, *Ticam1* (coding
136 for the TRIF adaptor), *Traf3* or *Irf3*, showed comparable levels of expression in the three
137 strains (Sup Fig 3B). Therefore, this analysis did not provide new clues for identifying the gene
138 responsible for the defect observed in CC071.
139 We then leveraged the genetic architecture of the CC which genomes are patchworks of
140 haplotypes inherited from the eight founder strains (17). Although CC071 was the only strain
141 with severe ZIKV disease, we hypothesized that, if the delayed activation of *Ifnb1* resulting in
142 uncontrolled viral replication observed in CC071 MEFs was due to an allele at one of the genes
143 involved in the *Ifnb1* induction pathway inherited from a parental strain, ZIKV-infected MEFs
144 of CC strains carrying the same allele would present similarly high viral titers. We therefore
145 derived MEFs from each available CC strain carrying the same ancestral haplotype as CC071
146 at one of the 13 genes of the pathway (Fig 2A). Upon ZIKV infection, none of these CC MEFs
147 showed viral titer kinetics resembling that observed in CC071 MEFs (Fig 2B). These results
148 suggested two alternative hypotheses. Either the delayed *Ifnb1* activation involved two
149 members of the pathway with a CC071-specific allelic combination resulting in non-functional
150 interaction, or CC071 was carrying a strain-specific allele at one of these genes, resulting from
151 a mutation that arose on an ancestral haplotype during the CC071 inbreeding. However, the

152 sequencing of one male of each CC strain reported in 2017 (18), did not identify such "private"
153 variants with high predicted impact in CC071 for any of these genes. Whatever the molecular
154 mechanism, our results indicated that it was specific to CC071.
155
156 *Genetic analysis identifies Irf3 as a candidate gene in a haplotype shared between CC071 and*
157 *CC001*
158 We then turned to a genetic mapping approach. We first established that (CC001xCC071)F1
159 MEFs responded to infection with rapid induction of *Ifnb1* expression, as CC001 (Sup Fig 4),
160 suggesting that the CC071 trait was recessively inherited. F1 mice were therefore backcrossed
161 with CC071. MEFs lines were produced from 51 backcross (BC) embryos, infected with ZIKV,
162 and analyzed for viral titer and *Ifnb1* expression as above. One CC001 and one CC071 MEF
163 lines were included in each infection experiment as controls. BC MEFs displayed either high
164 *Ifnb1* expression and low viral titer (like CC001), or high viral titer and delayed *Ifnb1* expression
165 (like CC071, Fig 3A-B), showing that these two traits correlated across the BC diverse genetic
166 backgrounds.
167 To confirm this apparently binary distribution, we conducted linear discriminant analysis (LDA)
168 on CC001 and CC071 MEFs using *Ifnb1* expression at the three time points. Applying the LDA
169 coefficients to backcross MEFs data classified individuals either in a CC001-like group (n=31;
170 61%) or in a CC071-like group (n=20; 39%), with a mean probability of 0.975 and 0.991,
171 respectively (Fig 3C). Quantitative trait locus (QTL) mapping was performed using LDA
172 classification as a binary trait. Genome scan identified a peak on chromosome 7 with a LOD
173 (logarithm of the odd) score of 9.138 ($p < 0.001$, Fig 4A) located in a region centered on the
174 *Irf3* gene which, given its main role in the regulation of *Ifnb1* expression, appeared as an
175 obvious candidate. However, both CC001 and CC071 inherited the CAST/EiJ haplotype in this
176 region (Fig 4B), strongly suggesting that CC071's defect was caused by a *de novo* mutation.
177
178 *Abnormal splicing of Irf3 mRNA in CC071 leads to a loss of function*
179 To identify the CC071-specific mutation, we re-analyzed the RNAseq data and investigated the
180 splicing events between *Irf3* exons. As shown in Fig 5A, no splicing was observed between
181 exons 6 and 7 in CC071 MEFs, while a short cryptic exon was added to exon 6 (red in Fig 5A).
182 This aberrant splicing resulted in an mRNA lacking the last two exons. Notably, exon 8 encodes
183 the serin-rich region of the protein with the phosphorylation sites necessary for IRF3

184 activation and nuclear translocation leading to *Ifnb1* transcription (Fig 5B). A combination of
185 long-range PCRs and sequencing did not identify the exact nature of *Irf3* genetic alteration in
186 CC071 but suggested the insertion of a repeated sequence between exons 6 and 7.
187 Nevertheless, the functional consequence of this mutation was confirmed by Western blot
188 using a specific C-terminal IRF3 antibody which showed that full-length IRF3 protein was
189 absent in CC071 MEFs (Fig 5C). Moreover, immunofluorescence using an antibody directed
190 against phosphorylated IRF3 detected a positive signal in the nucleus of many ZIKV-infected
191 CC001 and B6 MEFs, but not in CC071 MEFs (Fig 5D). Altogether, these results show that CC071
192 carries a mutation in *Irf3* that prevents IRF3 dimerization and phosphorylation which are
193 required to induce *Ifnb1* expression. Whether the altered mRNA sequence prevents the
194 production of the protein or alters its activity, this mutation results in IRF3 loss of function.
195
196 *Irf3 LOF is responsible for uncontrolled viral replication in CC071*
197 To test if the delayed *Ifnb1* expression resulting in uncontrolled viral replication in CC071 MEFs
198 was caused exclusively by *Irf3* LOF, we performed a quantitative complementation test by
199 producing compound heterozygous MEFs carrying a knockout *Irf3* allele ($Irf3^{KO}$) and the allele
200 from CC071 (denoted $Irf3^{KO}/Irf3^{71}$). These MEFs were compared with CC071 MEFs and with
201 heterozygous MEFs carrying a B6 wildtype allele and either an $Irf3^{KO}$ or an $Irf3^{71}$ allele
202 ($Irf3^{+}/Irf3^{KO}$ or $Irf3^{+}/Irf3^{71}$, respectively, Fig 6A). While $Irf3^{+}/Irf3^{KO}$ and $Irf3^{+}/Irf3^{71}$ ZIKV-infected
203 MEFs showed the same pattern as CC001 or B6 MEFs (rapid induction of *Ifnb1* expression and
204 controlled viral replication, see Fig 1A for comparison), CC071 and $Irf3^{KO}/Irf3^{71}$ MEFs carrying
205 two defective alleles at *Irf3* showed similar results (Fig 6B-C). These data demonstrate that,
206 since the $Irf3^{KO}$ did not complement the $Irf3^{71}$ allele, the *Irf3* mutation in CC071 contributes to
207 the defects observed in ZIKV-infected MEFs. Moreover, since the data obtained on CC071 and
208 on $Irf3^{KO}/Irf3^{71}$ MEFs were identical, we conclude that the *Irf3* mutation is sufficient to induce
209 the defects observed in CC071 MEFs.
210
211 *Irf3 LOF is not sufficient to explain CC071's susceptibility in vivo*
212 Lastly, we investigated whether the *Irf3* LOF was also responsible for the high susceptibility to
213 ZIKV of CC071 mice. We first compared clinical signs and plasma viral load in ZIKV-infected B6,
214 B6-$Irf3^{KO/KO}$ and CC071 mice pre-treated with MAR1-5A3. While no differences were observed
215 between B6 and B6-$Irf3^{KO/KO}$ (no clinical signs and moderate plasma viral loads), as expected

216 under conditions of neutralization of the IFN-I response, CC071 mice developed symptoms
217 (ruffled fur, hunched posture and body weight loss) around 7 days p.i. (Fig 7A), and
218 significantly higher viral loads at days 2 and 6 p.i. (Fig 7B) , indicating that genes not associated
219 to the IFN-I response play a major role in the susceptibility of CC071 mice to ZIKV infection.
220 We then measured plasma viral load in mice of the same genotypes infected without MAR1-
221 5A3 treatment. CC071 mice showed significantly higher viral loads at days 1 and 2 p.i., while
222 similar values were again observed in B6 and B6-*Irf3*$^{KO/KO}$ mice (Fig 7C). These results show
223 that, unlike at the cell level, *Irf3* LOF does not result in elevated viral replication in infected
224 mice (as measured by plasma viral load), either with or without IFNAR blockade, and therefore
225 is not sufficient to explain the high susceptibility of CC071 mice, suggesting the involvement
226 of other host genes.
227
228

229 **Discussion**

230 Among the CC strains we tested, CC071 mice pre-treated with anti-IFNAR antibody were the
231 most susceptible to ZIKV infection, with disease severity and peak plasma viral load almost as
232 high as those of B6-*Ifnar1* KO mice, and higher clinical signs and mortality than 129-*Ifnar1* KO
233 mice (15). In this susceptible model, IFN-I response is not permanently and ubiquitously
234 abrogated as in *Ifnar1* deficient strains, but delayed, temporarily blocked and not in tissues
235 unreached by the antibody (probably such as the brain). It is therefore particularly appropriate
236 to identify host susceptibility genes. However, traits measured *in vivo* such as viremia,
237 symptoms and death result from complex interactions between multiple pathways and cell
238 types, from which distinct mechanisms are difficult to dissect. Cultured MEFs offer a lower
239 level of complexity although they cannot provide the level of integration of a whole organism.
240 To decipher the susceptibility of CC071 mice, we used MEFs as a convenient cellular model
241 which can be easily derived from any mouse genetic background.

242 Starting from the confirmed observation of uncontrolled viral replication in CC071 MEFs, we
243 identified a delayed activation of the *Ifnb1* gene resulting in delayed stimulation of ISGs and
244 used a combination of genetic approaches to find the causative gene defect. The observation
245 that MEFs were normally responsive to IFN-I stimulation was consistent with the higher
246 susceptibility of mice treated by the MAR1-5A3 antibody compared with untreated mice (15).
247 These results pointed at the pathway from PAMP sensors to *Ifnb1* transcription factors.
248 Transcriptional analysis did not identify reduced expression of non-ISGs of this pathway. CC
249 strains' genomic structure allows searching for haplotypes inherited from the same founder
250 in CC strains showing similar phenotypes. However, we did not identify such haplotypes for
251 genes of the *Ifnb1* induction pathway, suggesting that the defects observed in CC071 MEFs
252 were strain-specific. It is finally the analysis of MEFs derived from backcross embryos that
253 established a monogenic inheritance, and genetic linkage unambiguously pointed at the
254 causative *Irf3* gene. The MEF experimental model was particularly appropriate since we could
255 derive cell lines from every backcross embryo. Our RNAseq data informed on the RNA splicing
256 defect in the *Irf3* gene, which functional consequences could be validated *in vitro*. The formal
257 proof that the CC071 *Irf3* mutation was necessary and sufficient to cause *Ifnb1* delayed
258 activation and uncontrolled viral replication came from a quantitative complementation test
259 using an *Irf3* KO allele.

260 Notably, this is not the first example of a *de novo* mutation responsible for a CC-strain-specific
261 trait. We (19) and others (20) previously reported the extreme susceptibility of CC042 to
262 *Salmonella* Typhimurium and to *Mycobacterium tuberculosis*, respectively, as a consequence
263 of a *de novo* 15-nucleotide deletion in the *Itgal1* gene. In the case of *Salmonella* Typhimurium,
264 CC042 was standing out, with bacterial loads up to 1000 times higher than other CC and the
265 susceptible B6 strains. In our previous study on ZIKV, CC071 was the most susceptible strain,
266 but its peak viral load was just the highest in a continuous distribution of values. Additionally,
267 this is not the first example of *Irf3* spontaneous polymorphism identified in mice modulating
268 susceptibility to bacterial (21) or viral infections (22).
269 *Irf3* is the main transcription factor involved in the innate immune response. It is constitutively
270 expressed and, at rest, inactive IRF3 is present in the cytoplasm. Upon viral entry (or other
271 stimuli that activate TLRs such as TLR3 and 4 or RIG-like receptors), signal transduction leads
272 to the phosphorylation of IRF3, leading to its dimerization and translocation to the nucleus
273 where it binds to the IFN-I genes promoters (23). This mechanism leads to the very fast
274 production of IFNβ which is secreted by the cell and triggers the immediate response to viral
275 infection through the activation of ISGs with diverse antiviral functions (24). In humans, LOF
276 mutations in *Irf3* have been associated with increased susceptibility to West Nile virus (WNV)
277 (25, 26), herpes simplex virus 1 (HSV-1) (27, 28) and more recently to SARS-CoV-2 (29).
278 In mice, many studies have used *Irf3*-deficient models. After infection with WNV, viral
279 replication was increased in *Irf3*$^{KO/KO}$ bone marrow macrophages (BMMs) and primary neurons
280 (30). Higher viral replication was observed in HSV-1-infected *Irf3*$^{KO/KO}$ bone marrow-derived
281 dendritic cells (BMDCs) and BMMs, and IFNβ was reduced in BMDCs supernatants (31).
282 Similarly, *Ifnb1* expression was reduced in HSV-1-infected (32) and CHIKV-infected (33)
283 *Irf3*$^{KO/KO}$ MEFs. In line with these findings, our study provides, to our knowledge, the first
284 evidence for a role of *Irf3* in the infection of murine cells by ZIKV.
285 *In vivo* studies led to contrasting results depending on the virus and infection route. *Irf3*$^{KO/KO}$
286 mice were reported to be resistant to ZIKV with no mortality nor body weight loss (10).
287 Moreover, we found that plasma viral loads were similar in B6-*Irf3*$^{KO/KO}$ and B6 mice, whether
288 mice were treated with anti-IFNAR antibody, or not. Likewise, *Irf3*$^{KO/KO}$ mice showed no
289 mortality and low virus in the circulation following dengue virus (34) and CHIKV infection (33).
290 Contrastingly, WNV infection was lethal in *Irf3*$^{KO/KO}$ mice while 65% of infected WT mice
291 survived, suggesting that *Irf3* LOF may impact clinical parameters (survival, body weight loss)

292 only in the case of highly pathogenic viruses. The route of infection may also be a critical
293 parameter. After intravenous inoculation with HSV-1, all WT and *Irf3*$^{KO/KO}$ mice survived (32),
294 while intranasal inoculation led to 30% and 90% mortality in WT and *Irf3*$^{KO/KO}$ mice,
295 respectively (35).
296 Our *in vivo* data showing higher viral load in CC071 than in B6-*Irf3*$^{KO/KO}$ mice, with clinical signs,
297 indicate that other genes control the susceptibility of CC071. The results of the
298 complementation test on MEFs, with CC071 and *Irf3*^{KO}/*Irf3*^{71} yielding very similar data, suggest
299 that these genes may not act at the cell level, at least during the first 72 hpi. Our poor
300 understanding of the severe disease developing in CC071 ZIKV-infected mice does not point
301 at potential mechanisms. As in this study, appropriate crosses will be necessary to detect
302 genomic regions from which candidate genes could be identified and validated. It will then be
303 possible to assess the specific contribution of the *Irf3* LOF mutation to the susceptibility of
304 CC071 mice.
305 CC071 has been reported to be susceptible to other flaviviruses. High viral load was found
306 after dengue infection (15). Lethality after infection with WNV (15) or Powassan virus (36)
307 were also described, although there is likely contribution from the defective *Oas1b* allele that
308 CC071 has inherited from 129S1/SvImJ. CC071 was also one of the most susceptible CC strains
309 to Rift Valley Fever virus infection (37) and to hepacivirus, with long-term viral persistence
310 (38). Because of its unique genetic background, this strain will be increasingly useful for
311 infectious disease studies, which justifies deciphering its mechanisms of susceptibility.
312

313 **Material and methods**

314

315 *Mice and crosses*

316 C57BL/6J mice were purchased from Charles River Laboratories France. Collaborative Cross
317 strains (CC001/Unc, CC071/TauUnc, CC005/TauUnc, CC011/Unc, CC026/GeniUnc,
318 CC061/GeniUnc, CC021/Unc, CC006/TauUnc, CC025/GeniUnc, CC039/Unc, CC060/Unc) were
319 purchased from the Systems Genetics Core Facility, University of North Carolina and bred at
320 the Institut Pasteur. *Irf3 Irf7* double KO mice (C57BL/6J-*Bcl2l12*/*Irf3*^{tm1Ttg} *Irf7*^{tm1Ttg},(32, 39); B6-
321 *Irf3*^{KO} and B6-*Irf7*^{KO} thereafter) were bred at the Institut Pasteur. All mice were maintained as
322 described previously (15). (CC001 x CC071) x CC071 backcross embryos were obtained from
323 reciprocal crosses (F1 female x CC071 male and vice-versa). For the quantitative
324 complementation test, B6-*Irf3*$^{+/KO}$ B6-*Irf7*$^{+/KO}$ females were crossed with CC071 males and B6-
325 *Irf3*$^{+/KO}$ B6-*Irf7*$^{+/KO}$ males were crossed with C57BL/6J females. Genotype at the *Irf7* loci was
326 not considered as only B6-*Irf7*$^{+/KO}$ of B6-*Irf7*$^{+/+}$ mice were used. For *in vivo* infections, B6-*Irf3*
327 simple KO mice were obtained from an F2 between B6-*Irf3 Irf7* double KO and B6 mice. Mouse
328 experiments were approved by the Institut Pasteur Ethics Committee and authorized by the
329 French Ministry of Research (project #19469), in compliance with French and European
330 regulations.

331

332 *ZIKA virus*

333 The FG15 Asian Zika virus (ZIKV) strain, isolated from a patient during ZIKV outbreak in French
334 Guiana in December 2015, was obtained from the Virology Laboratory of the Institut Pasteur
335 of French Guiana. Viral stock (passage 5) was prepared from supernatant of infected C6/36
336 cells, clarified by centrifugation at 800g and titrated on Vero cells by focus-forming assay.

337

338 *Mouse infection*

339 All infection experiments were performed in a biosafety level 3 animal facility and mice were
340 kept in isolators. Six- to 10-week-old, male or female mice were injected intraperitoneally with
341 10^7 PFU of ZIKV FG15. Mice received an IP injection of 2 mg of MAR1-5A3 anti-IFNAR antibody
342 (Euromedex, Cat#BX-BE0241) one day prior infection. Mouse numbers are indicated in figure
343 legends. Both males and females were used since no differences between sexes were
344 detected in our previous and present experiments. Clinical signs and body weight loss were

345 recorded for up to seven days post infection. Blood samples were collected on EDTA at two-
346 and six-days post infection from the retromandibular vein for plasma viral load assessment.
347 Quantification of ZIKV viral copies by qPCR was previously described (15).
348 *MEFs isolation*
349 Pregnant females were euthanized at day 13.5-15.5 of gestation. For B6, CC001 and CC071,
350 MEFs were isolated from individual fetuses to obtain biological replicates. For other CC strains,
351 MEFs were derived from individual or pooled fetuses. Fetus bodies were chopped and
352 digested with trypsin (Gibco Cat#25300054), then cultured at 37°C and 5% CO_2 in complete
353 medium (DMEM Gibco Cat# 31966047, 10% fetal bovine serum PAA Laboratories Cat#A15-
354 101, 1% penicillin/streptomycin Sigma Cat#P4333). MEFs were used until passage 2. For the
355 backcross experiment, MEF lines were isolated from 52 backcross fetuses. Heads were used
356 to prepare DNA for whole-genome genotyping.
357
358 *MEFs infection*
359 MEFs were seeded at 5.10^4 cells per well in 24-well plates the day before infection. They were
360 exposed to ZIKV FG15 strain at a MOI of 5 for 2 hours after which the inoculum was replaced
361 with fresh complete medium and MEFs were incubated for up to 72 hours. For kinetics studies,
362 different wells were used for each time point. Backcross MEFs were infected in 6 infection
363 experiments, each of which included a CC001 and a CC071 MEF lines.
364
365 *MEFs IFNα stimulation*
366 MEFs were seeded at 5.10^4 cells per well in 24-well plates the day before stimulation and
367 treated with 300 IU/mL IFNα (Miltenyi Biotec Cat#130-093-131) and incubated for up to 24
368 hours.
369
370 *Focus forming assay*
371 Quantification of ZIKV particles was completed by focus forming assay on Vero cells (ATCC
372 CRL-1586) as previously described (15).
373
374 *RNA extraction from cells*

375 MEFs were lysed in 350µL of RLT buffer (Qiagen) with 1% β-mercaptoethanol. RNA was
376 extracted using RNeasy Mini Kit (Qiagen Cat#74104) according to the manufacturer's
377 instructions, with DNase I (Qiagen Cat# 79254) to prevent genomic DNA contamination.
378
379 *Reverse transcription and qPCR*
380 Reverse-transcription was performed on 200ng of RNA using Superscript II polymerase
381 (Invitrogen Cat#18064022) RNaseOUT ribonuclease inhibitor (Invitrogen Cat#10777019).
382 qPCR was performed on 20ng of cDNAs using Power SYBR Green PCR Master Mix (Applied
383 Biosystems Cat#4367659) and 6pmol of each primer, on a QuantStudio 12K Flex or a ViiA 7
384 (ThermoFisher Scientific). Primers (Eurofins) sequences are provided in Sup Table 1. Gene
385 expression was expressed on a Log10 scale of relative expression to the reference *Tbp* gene.
386
387 *Genotyping*
388 Genomic DNA was prepared from backcross fetuses' heads by proteinase K digestion, phenol-
389 chloroform extraction and ethanol precipitation according to standard protocols. DNAs were
390 sent to Neogen (Neogen/Geneseek, Inc, Lincoln, NE, USA) for whole-genome genotyping using
391 the MiniMUGA array containing 11,125 SNP markers. For the quantitative complementation
392 test, *Irf3* and *Irf7* genotyping was performed by Transnetyx (Cordova, TN) by real-time PCR on
393 fetuses' heads.
394
395 *RNA splicing analysis from RNA sequencing data*
396 RNA sequencing data were produced as described in the Supplementary methods. Splicing
397 analysis was performed using Majiq 2.4 (40) with default parameters to investigate alternative
398 transcripts between conditions, focusing on the *Irf3* gene.
399
400 *Immunofluorescence*
401 MEFs were plated on glass coverslips before infection, fixed with 4% paraformaldehyde for 20
402 min and permeabilized with pure methanol for 10min at -20°C. Cells were incubated with
403 blocking buffer (5% FBS 0.3% triton in PBS) for 1 hour, with primary antibodies diluted in
404 antibody incubation buffer (AIB: 1% BSA 0.3% triton in PBS) overnight at 4°C and with
405 secondary antibodies and Hoechst (dilution 1:1000) diluted in AIB for 1 hour. Coverslips were
406 mounted on slides and imaged with a widefield microscope (Zeiss Axio Observer.Z1 with a

407 Plan-Apochromat 20x/0.8 M27 objective and a Hamamatsu sCMOS ORCA-Flash 4.0 v3
408 camera). ZEN blue 2012 software (ZEISS) imaging software was used for image capture and
409 Image J software (National Institutes of Health) to adjust brightness and contrast. Primary and
410 secondary antibodies are indicated in Sup Table 2.
411
412 *Western blot*
413 MEFs were trypsinized for 5 min, washed and lysed in a protein extraction buffer (10mM
414 TrisHCl pH7.5, 5mM EDTA, 150mM NaCl, 30mM Na_2HPO_4, 50mM NaF, 10% glycerol, 1% NP40,
415 1X cOmplete (Roche #11873580001), 1X PhosSTOP (Roche #4906845001), 1/1000 benzonaze
416 (Sigma Cat#E1014)) for 30 min at 4°C. Proteins diluted in Laemmli were resolved on 4-12% Bis-
417 Tris gels (Invitrogen Cat#NP0323BOX) in MOPS buffer (Invitrogen Cat#NP0001) and
418 transferred to nitrocellulose membranes (Bio-Rad Cat#1620112) in a 25mM Tris 200mM
419 glycine 20% ethanol buffer. Blots were blocked in 5% milk in TBS-T (0.1% Tween20 in Tris Base
420 Sodium), incubated with primary antibodies diluted in 3% milk in TBST overnight at 4°C, and
421 incubated with secondary antibodies diluted in 3% milk in TBST for 90 min. Blots were revealed
422 with ECL substrate (Thermo Scientific Cat#32132) and imaged with X-ray films. Primary and
423 secondary antibodies are indicated in Sup Table 2.
424
425 *Statistical analysis*
426 Statistical analyses were performed using R (41) version 4.1.0. Viral titers, gene expression
427 and genome copies were Log10-transformed for graphs and statistical tests. One way ANOVA
428 followed by Tukey HSD were used for testing multiple comparisons. For *in vivo* studies, non-
429 parametric Kruskal-Wallis followed by Wilcoxon tests with Bonferroni correction for multiple
430 testing were used to handle values below the limit of detection. Linear discriminant analysis
431 (LDA) was conducted using the MASS package (42). The LDA was trained on the phenotypes
432 of the two parental CC001 and CC071 strains from each infection batch. LDA coefficients were
433 applied to backcross mice for assignment to "CC071-like" or "CC001-like" groups.
434
435 *Genetic analysis*
436 Raw genotypes were curated using the stuart package (43). QTL mapping was performed using
437 R/qtl (44). LDA prediction was used as a binary trait. Statistical significance thresholds were

438 computed by data permutation (n=1000). 95% confidence interval was estimated using the
439 Bayesian method.

Acknowledgements

We thank Matthieu Prot, Maxime Chazal and Sandrine Vandormael-Pournin for technical advice and for providing reagents. We are grateful to Tommy Penel and Rachid Chennouf of the Institut Pasteur Central Animal Facility of the C2RA (Center for Animal Resources and Research) for the careful breeding of CC strains and for the maintenance of mice in the BSL-3 animal facility, respectively. We thank Etienne Simon-Loriere and Nolwenn Jouvenet for scientific advice and continuous support along this project.

Author contributions

X.M. conceived and supervised this study. M.B. and C.M. designed and performed the experiments and analyzed data. L.C. and C.R.P. performed experiments. E.K. analyzed RNAseq data. X.M. designed experiments and analyzed data. E.B. provided conceptual advice. M.B., C.M. and X.M. wrote the paper. All authors commented on and edited the manuscript.

Funding

This work was supported by grants from the Agence Nationale de la Recherche (ANR) NeuroZika (ANR-20-CE16-0017) and from the French Government's Investissement d'Avenir program, Laboratoire d'Excellence: IBEID (Integrative Biology of Emerging Infectious Diseases, ANR-10-LABX-62-IBEID). C.M. and M.B. were supported by doctoral fellowships from grant ANR-10-LABX-62-IBEID.

Availability of data and materials

RNAseq primary data are available from the European Nucleotide Archive (accession number E-MTAB-12765). All other experimental data that support the finding of this study are available from the corresponding authors upon reasonable request.

Competing interests

The authors declare that they have no competing interests.

470

471 **Figure legends**

472

473 **Figure 1. CC071 MEFs fail to control viral replication, with delayed *Ifnb1* expression but**
474 **normal response to IFN-I.** (A,B) MEFs derived from B6 (black circles), CC001 (blue triangles)
475 and CC071 (red squares) were infected with ZIKV at a MOI of 5 and analyzed 24, 48 and 72 hpi
476 (A) Viral titer in supernatants was quantified by FFA. (B) *Ifnb1* expression was normalized to
477 *Tbp* reference gene. Data are mean +/- sem from 3 to 4 biological replicates per strain (MEFs
478 derived from individual embryos). (C) MEFs were stimulated with recombinant IFNα. *Ifitm3*
479 relative expression normalized to *Tbp* reference gene is shown as an example of ISG. Data are
480 mean +/- sem from 2 to 3 biological replicates. Blue asterisks and black hashes show statistical
481 significance of CC071 compared to CC001 and to B6, respectively (ANOVA followed by Tukey
482 HSD, */# $p < 0.05$, **/## $p < 0.01$, *** $p < 0.001$).

483

484 **Figure 2. Haplotype analysis fails to identify a genes from the IFN-I induction pathway**
485 **associated with uncontrolled viral replication.** (A) Identification of CC strains which carry the
486 same ancestral haplotype as CC071 at the genes involved in the pathway leading to IFN-I
487 expression. Colored boxes indicate matched haplotypes between CC071 and other CC strains.
488 Letters and colors designate the eight CC founder strains. A: A/J (yellow); B: C57BL/6J; C:
489 129S1/SvImJ (pink); D: NOD/ShiLtJ; E: NZO/HILtJ (light blue); F: CAST/EiJ (green); G: PWK/PhJ
490 (red); H: WSB/EiJ (purple). Doubled letters (eg AA) indicate homozygous genotypes.
491 Heterozygous genotypes are indicated by the two corresponding letters (eg AD). (B) Kinetics
492 of viral titer in MEFs from CC071 and the 8 CC strains shown in (A). Experimental conditions
493 were as in Figure 1A. n: number of technical replicates for each strain. Data are mean +/- sem
494 from the technical replicates. Letters show statistical significance between CC071 and other
495 strains. (ANOVA followed by Tukey HSD, a: $p < 0.05$, b: $p < 0.01$, c: $p < 0.001$).

496

497 **Figure 3. Backcross MEFs display either a CC001-like or a CC071-like phenotype.** MEFs
498 derived from CC001 (blue triangles), CC071 (red squares) and backcross (gray circles) embryos
499 were infected with ZIKV at a MOI of 5. (A) Viral titer and (B) *Ifnb1* expression in ZIKV-infected
500 MEFs from 9 backcross embryos. Experimental conditions were as in Figure 1A-B. Red and
501 blue curves show the results for CC071 and CC001 MEFs, respectively, from the same infection

502 experiment. (C) Results of LDA on the backcross MEFs. LDA coefficients were calculated from
503 *Ifnb1* expression data in CC001 and CC071 infected MEFs and applied to backcross MEFs. The
504 graph shows the probability of each BC MEF to belong to the "CC001-like" group, resulting in
505 two distinct populations shown in blue ("CC001-like") and in red ("CC071-like"). n: number of
506 BC MEFs assigned to each group.
507
508 **Figure 4. Genetic analysis of *Ifnb1* expression in backcross MEFs identifies a major**
509 **determinant mapping to the *Irf3* locus.** (A) Genome-wide linkage analysis of the LDA
510 classification of backcross MEFs performed with R/qtl. X-axis: genomic location. Y-axis: LOD
511 score of the phenotype-genotype association. Genome-wide significance thresholds (P = 0.05,
512 P = 0.1 and P = 0.63) were computed from 1000 data permutation. The chromosome 7 peak
513 has a LOD score of 9.138. (B) Schematic representation of CC001 and CC071 chromosome 7
514 haplotypes, from https://csbio.unc.edu/CCstatus/CCGenomes/. Colors represent the CC
515 ancestral haplotypes (same colors as in Figure 2A). Thick vertical black lines show the peak's
516 95% Bayesian confidence interval (25.9-31.3 cM, corresponding to 40.1-50.6 Mb). The red line
517 shows the position of *Irf3* gene.
518
519 **Figure 5. CC071 *Irf3* mRNAs show abnormal splicing, resulting in defective IRF3 protein.** (A)
520 Schematic representation of the exons of the *Irf3* gene with the number of reads spanning
521 successive exons in the CC001 and CC071 RNAseq data (one sample of each strain). The red
522 box between CC071's exons 6 and 7 depicts a novel exon resulting from abnormal splicing. (B)
523 Schematic representation of the IRF3 protein structural domains (exon 1 is untranslated). Exon
524 8 encodes the serine rich region containing the phosphorylation sites for IRF3 activation. (C)
525 Western blot using an anti-C-terminal IRF3 antibody from mock-infected and ZIKV-infected
526 B6, CC001 and CC071 MEFs at 2 hpi, showing the absence of full-length IRF3 in CC071 MEFs.
527 Vinculin was used as a loading control. (D) Immunofluorescence using an anti-phosphorylated
528 IRF3 (pIRF3, green) in ZIKV-infected B6, CC001 and CC071 MEFs at 24 hpi, showing the absence
529 of pIRF3 in the nucleus of CC071 MEFs upon infection. Red-labeled 4G2 antibody labels ZIKV-
530 infected cells. Cell nuclear DNA labeled by Hoechst (blue). Quantification of the number of
531 infected and pIRF3 positive cells is presented in the table. Proportions were established on
532 420, 428 and 551 cells for CC001, CC071 and B6, respectively.
533

534 **Figure 6. Quantitative complementation test confirms that *Irf3* LOF in CC071 is responsible**
535 **for uncontrolled viral replication and delayed *Ifnb1* expression.** (A) Mice heterozygous for an
536 inactivated *Irf3* allele (B6-$Irf3^{+}$/$Irf3^{KO}$) were mated with B6 and with CC071 mice to produce
537 four types of embryos from which MEFs were derived. The genetic background and *Irf3*
538 genotype is shown below each type of embryos. (B) Viral titer and (C) *Ifnb1* expression in ZIKV-
539 infected MEFs. Experimental conditions were as in Figure 1A-B. Data are mean +/- sem from
540 3 biological replicates for each group. At every time point, the comparison of either CC071 or
541 $Irf3^{KO}$/$Irf3^{71}$ with either $Irf3^{+}$/$Irf3^{71}$ or $Irf3^{+}$/$Irf3^{KO}$ gave identical statistical significance (ANOVA
542 followed by post-hoc Tukey HSD, * $p < 0.05$, ** $p < 0.01$, *** $p < 0.001$).
543
544 **Figure 7. *Irf3* LOF is not sufficient to explain CC071 susceptibility to ZIKV infection *in vivo*.**
545 CC071, B6-$Irf3^{KO}$ and B6 mice were infected IP with 10^7 FFUs of ZIKV and monitored for 7 days,
546 with (A,B) or without (C) IP injection of 2 mg of MAR1-5A3 IFNAR-blocking monoclonal
547 antibody 24 h before infection. (A) Average clinical score of anti-IFNAR-treated at day 6 p.i.
548 (B,C) Plasma viral load measured by RT-qPCR. Each dot represents one mouse. Groups were
549 compared by Kruskal-Wallis test followed by Wilcoxon test with Bonferroni correction for
550 multiple testing (* $p < 0.05$).
551
552

553 **Supplemental information**

554

555 **Legend to supplemental figures**

556

557 **Figure S1. *Ifna4* expression is delayed in ZIKV-infected CC071 MEFs.** MEFs derived from B6
558 (gray circles), CC001 (blue triangles) and CC071 (red squares) were infected with ZIKV at a MOI
559 of 5. *Ifna4* expression was determined by RT-qPCR on MEFs total RNA by normalizing to *Tbp*
560 housekeeping gene. Data are mean +/- sem from 3 biological replicates. One CC001, one B6
561 and one CC071 replicates at 0 hpi and one CC071 replicate at 24 hpi were below the limit of
562 detection. Blue asterisks and black hashes show statistical significance of CC071 compared to
563 CC001 and to B6, respectively (ANOVA followed by post-hoc Tukey HSD, */# $p < 0.05$, *** $p <$
564 0.001).

565

566 **Figure S2. Delayed IFN-I expression in CC071 MEFs results from a constitutive defect in**
567 **innate antiviral response.** MEFs were transfected with either (A) poly(I:C), which activates
568 both TLR and RIG-I pathways, or (B) 3p-hpRNA, a RIG-I agonist. *Ifnb1* expression was
569 determined as in Figure 1B. Data are mean +/- sem from 3 biological replicates for CC001 and
570 CC071 (2 at 4 hours) or 2 biological replicates for B6 (1 at 4 hours). Blue asterisks and black
571 hashes show statistical significance of CC071 compared to CC001 and to B6, respectively
572 (ANOVA followed by post-hoc Tukey HSD, */# $p < 0.05$).

573

574 **Figure S3**. **Expression of genes involved in the *Ifnb1* induction pathway in ZIKV-infected MEFs**
575 **of B6, CC001 and CC071 strains.** MEFs derived from B6 (black circles), CC001 (blue triangles)
576 and CC071 (red squares) were infected with ZIKV at a MOI of 5. mRNA expression levels were
577 measured by RNAseq in non-infected (NI) and ZIKV-infected MEFs. (A) Number of upregulated
578 genes per strain at 16, 24 and 32 hpi (B-G) Genes constitutively expressed. (H-N) Genes which
579 expression is induced by the IFN-I response (ISGs). Expression levels are shown on a
580 logarithmic scale. For *Ifnb1* expression, null counts were transformed to 1. Data are mean +/-
581 sem from 3 biological replicates. Blue asterisks and black hashes show statistical significance
582 of CC071 compared to CC001 to B6, respectively (ANOVA followed by post-hoc Tukey HSD,
583 */# $p < 0.05$, **/## $p < 0.01$, ***/### $p < 0.001$).

584

585 **Figure S4. (CC001xCC071)F1 MEFs show normal induction of *Ifnb1*.** *Ifnb1* expression upon
586 ZIKV infection in CC001, CC071 and (CC001xCC071)F1 MEFs determined as in Figure 1B. Data
587 are mean +/- sem from 3 biological replicates. Blue asterisks and orange hashes show
588 statistical significance of CC071 compared to CC001 and to F1, respectively (ANOVA followed
589 by post-hoc Tukey HSD, **/## $p < 0.01$).
590

591 **References**

592 1. Cao-Lormeau V-M, Blake A, Mons S, Lastère S, Roche C, Vanhomwegen J, Dub T,
593 Baudouin L, Teissier A, Larre P, Vial A-L, Decam C, Choumet V, Halstead SK, Willison HJ,
594 Musset L, Manuguerra J-C, Despres P, Fournier E, Mallet H-P, Musso D, Fontanet A, Neil
595 J, Ghawché F. 2016. Guillain-Barré Syndrome outbreak associated with Zika virus
596 infection in French Polynesia: a case-control study. Lancet 387:1531–1539.

597 2. Carod-Artal FJ. 2018. Neurological complications of Zika virus infection. Expert Review of
598 Anti-infective Therapy 16:399–410.

599 3. Oliveira Melo AS, Malinger G, Ximenes R, Szejnfeld PO, Alves Sampaio S, Bispo de Filippis
600 AM. 2016. Zika virus intrauterine infection causes fetal brain abnormality and
601 microcephaly: tip of the iceberg?: Physician Alert. Ultrasound Obstet Gynecol 47:6–7.

602 4. Paixao ES, Cardim LL, Costa MCN, Brickley EB, de Carvalho-Sauer RCO, Carmo EH,
603 Andrade RFS, Rodrigues MS, Veiga RV, Costa LC, Moore CA, França GVA, Smeeth L,
604 Rodrigues LC, Barreto ML, Teixeira MG. 2022. Mortality from Congenital Zika Syndrome
605 — Nationwide Cohort Study in Brazil. N Engl J Med 386:757–767.

606 5. Rossi SL, Ebel GD, Shan C, Shi P-Y, Vasilakis N. 2018. Did Zika Virus Mutate to Cause Severe
607 Outbreaks? Trends in Microbiology 26:877–885.

608 6. Liu Z-Y, Shi W-F, Qin C-F. 2019. The evolution of Zika virus from Asia to the Americas. Nat
609 Rev Microbiol 17:131–139.

610 7. Manet C, Roth C, Tawfik A, Cantaert T, Sakuntabhai A, Montagutelli X. 2018. Host genetic
611 control of mosquito-borne Flavivirus infections. Mamm Genome 29:384–407.

612 8. Rasmussen AL, Okumura A, Ferris MT, Green R, Feldmann F, Kelly SM, Scott DP, Safronetz
613 D, Haddock E, LaCasse R, Thomas MJ, Sova P, Carter VS, Weiss JM, Miller DR, Shaw GD,
614 Korth MJ, Heise MT, Baric RS, de Villena FP-M, Feldmann H, Katze MG. 2014. Host genetic
615 diversity enables Ebola hemorrhagic fever pathogenesis and resistance. Science
616 346:987–991.

617 9. Gralinski LE, Menachery VD, Morgan AP, Totura AL, Beall A, Kocher J, Plante J, Harrison-
618 Shostak DC, Schafer A, Pardo-Manuel de Villena F, Ferris MT, Baric RS. 2017. Allelic
619 Variation in the Toll-Like Receptor Adaptor Protein Ticam2 Contributes to SARS-
620 Coronavirus Pathogenesis in Mice. G3 (Bethesda) 7:1653–1663.

621 10. Lazear HM, Govero J, Smith AM, Platt DJ, Fernandez E, Miner JJ, Diamond MS. 2016. A
622 Mouse Model of Zika Virus Pathogenesis. Cell Host Microbe 19:720–730.

623 11. Grant A, Ponia SS, Tripathi S, Balasubramaniam V, Miorin L, Sourisseau M, Schwarz MC,
624 Sánchez-Seco MP, Evans MJ, Best SM, García-Sastre A. 2016. Zika Virus Targets Human
625 STAT2 to Inhibit Type I Interferon Signaling. Cell Host & Microbe 19:882–890.

626 12. Sheehan KCF, Lai KS, Dunn GP, Bruce AT, Diamond MS, Heutel JD, Dungo-Arthur C,
627 Carrero JA, White JM, Hertzog PJ, Schreiber RD. 2006. Blocking Monoclonal Antibodies
628 Specific for Mouse IFN- *α* / *β* Receptor Subunit 1 (IFNAR-1) from Mice Immunized by *In*
629 *Vivo* Hydrodynamic Transfection. Journal of Interferon & Cytokine Research 26:804–819.

630 13. Roberts A, Pardo-Manuel de Villena F, Wang W, McMillan L, Threadgill DW. 2007. The
631 polymorphism architecture of mouse genetic resources elucidated using genome-wide
632 resequencing data: implications for QTL discovery and systems genetics. Mamm Genome
633 18:473–481.

634 14. Keane TM, Goodstadt L, Danecek P, White MA, Wong K, Yalcin B, Heger A, Agam A, Slater
635 G, Goodson M, Furlotte NA, Eskin E, Nellåker C, Whitley H, Cleak J, Janowitz D,
636 Hernandez-Pliego P, Edwards A, Belgard TG, Oliver PL, McIntyre RE, Bhomra A, Nicod J,
637 Gan X, Yuan W, van der Weyden L, Steward CA, Bala S, Stalker J, Mott R, Durbin R, Jackson
638 IJ, Czechanski A, Guerra-Assunção JA, Donahue LR, Reinholdt LG, Payseur BA, Ponting CP,
639 Birney E, Flint J, Adams DJ. 2011. Mouse genomic variation and its effect on phenotypes
640 and gene regulation. Nature 477:289–294.

641 15. Manet C, Simon-Lorière E, Jouvion G, Hardy D, Prot M, Conquet L, Flamand M, Panthier
642 J-J, Sakuntabhai A, Montagutelli X. 2020. Genetic Diversity of Collaborative Cross Mice
643 Controls Viral Replication, Clinical Severity, and Brain Pathology Induced by Zika Virus
644 Infection, Independently of Oas1b. J Virol 94.

645 16. McCartney S, Vermi W, Gilfillan S, Cella M, Murphy TL, Schreiber RD, Murphy KM,
646 Colonna M. 2009. Distinct and complementary functions of MDA5 and TLR3 in poly(I:C)-
647 mediated activation of mouse NK cells. Journal of Experimental Medicine 206:2967–
648 2976.

649 17. Collaborative Cross Consortium. 2012. The Genome Architecture of the Collaborative
650 Cross Mouse Genetic Reference Population. Genetics 190:389–401.

651 18. Srivastava A, Morgan AP, Najarian ML, Sarsani VK, Sigmon JS, Shorter JR, Kashfeen A,
652 McMullan RC, Williams LH, Giusti-Rodríguez P, Ferris MT, Sullivan P, Hock P, Miller DR,
653 Bell TA, McMillan L, Churchill GA, Villena FP-M de. 2017. Genomes of the Mouse
654 Collaborative Cross. Genetics 206:537–556.

655 19. Zhang J, Teh M, Kim J, Eva MM, Cayrol R, Meade R, Nijnik A, Montagutelli X, Malo D,
656 Jaubert J. 2019. A Loss-of-Function Mutation in the Integrin Alpha L (Itgal) Gene
657 Contributes to Susceptibility to Salmonella enterica Serovar Typhimurium Infection in
658 Collaborative Cross Strain CC042. Infect Immun 88.

659 20. Smith CM, Proulx MK, Lai R, Kiritsy MC, Bell TA, Hock P, Pardo-Manuel de Villena F, Ferris
660 MT, Baker RE, Behar SM, Sassetti CM. 2019. Functionally Overlapping Variants Control
661 Tuberculosis Susceptibility in Collaborative Cross Mice. mBio 10:e02791-19.

662 21. Garifulin O, Qi Z, Shen H, Patnala S, Green MR, Boyartchuk V. 2007. Irf3 Polymorphism
663 Alters Induction of Interferon Beta in Response to Listeria monocytogenes Infection.
664 PLOS Genetics 3:e152.

665 22. Moore TC, Al-Salleeh FM, Brown DM, Petro TM. 2011. IRF3 polymorphisms induce
666 different innate anti-Theiler's virus immune responses in RAW264.7 macrophages.
667 Virology 418:40–48.

668 23. Bourdon M, Manet C, Montagutelli X. 2020. Host genetic susceptibility to viral infections:
669 the role of type I interferon induction. Genes Immun 21:365–379.

670 24. Schoggins JW. 2019. Interferon-Stimulated Genes: What Do They All Do? Annu Rev Virol
671 6:567–584.

672 25. Bigham AW, Buckingham KJ, Husain S, Emond MJ, Bofferding KM, Gildersleeve H,
673 Rutherford A, Astakhova NM, Perelygin AA, Busch MP, Murray KO, Sejvar JJ, Green S,
674 Kriesel J, Brinton MA, Bamshad M. 2011. Host genetic risk factors for West Nile virus
675 infection and disease progression. PLoS One 6:e24745.

676 26. Cahill ME, Conley S, DeWan AT, Montgomery RR. 2018. Identification of genetic variants
677 associated with dengue or West Nile virus disease: a systematic review and meta-
678 analysis. BMC Infect Dis 18:282.

679 27. Mork N, Kofod-Olsen E, Sorensen KB, Bach E, Orntoft TF, Ostergaard L, Paludan SR,
680 Christiansen M, Mogensen TH. 2015. Mutations in the TLR3 signaling pathway and
681 beyond in adult patients with herpes simplex encephalitis. Genes Immun 16:552–66.

682 28. Andersen LL, Mork N, Reinert LS, Kofod-Olsen E, Narita R, Jorgensen SE, Skipper KA,
683 Honing K, Gad HH, Ostergaard L, Orntoft TF, Hornung V, Paludan SR, Mikkelsen JG, Fujita
684 T, Christiansen M, Hartmann R, Mogensen TH. 2015. Functional IRF3 deficiency in a
685 patient with herpes simplex encephalitis. J Exp Med 212:1371–9.

686 29. Zhang Q, Bastard P, Liu Z, Le Pen J, Moncada-Velez M, Chen J, Ogishi M, Sabli IKD, Hodeib
687 S, Korol C, Rosain J, Bilguvar K, Ye J, Bolze A, Bigio B, Yang R, Arias AA, Zhou Q, Zhang Y,
688 Onodi F, Korniotis S, Karpf L, Philippot Q, Chbihi M, Bonnet-Madin L, Dorgham K, Smith
689 N, Schneider WM, Razooky BS, Hoffmann HH, Michailidis E, Moens L, Han JE, Lorenzo L,
690 Bizien L, Meade P, Neehus AL, Ugurbil AC, Corneau A, Kerner G, Zhang P, Rapaport F,
691 Seeleuthner Y, Manry J, Masson C, Schmitt Y, Schluter A, Le Voyer T, Khan T, Li J, Fellay J,
692 Roussel L, Shahrooei M, Alosaimi MF, Mansouri D, Al-Saud H, Al-Mulla F, Almourfi F, Al-
693 Muhsen SZ, Alsohime F, Al Turki S, Hasanato R, van de Beek D, Biondi A, Bettini LR,
694 D'Angio M, Bonfanti P, Imberti L, Sottini A, Paghera S, Quiros-Roldan E, Rossi C, Oler AJ,
695 Tompkins MF, Alba C, Vandernoot I, Goffard JC, Smits G, Migeotte I, Haerynck F, Soler-
696 Palacin P, Martin-Nalda A, Colobran R, Morange PE, Keles S, Colkesen F, Ozcelik T, Yasar
697 KK, Senoglu S, Karabela SN, Gallego CR, Novelli G, Hraiech S, Tandjaoui-Lambiotte Y,
698 Duval X, Laouenan C, Clinicians C-S, Clinicians C, Imagine CG, French CCSG, Co VCC,

699 Amsterdam UMCC, Biobank, Effort CHG, Niaid U, Group TCI, Snow AL, Dalgard CL, Milner
700 J, Vinh DC, Mogensen TH, Marr N, Spaan AN, Boisson B, Boisson-Dupuis S, Bustamante J,
701 Puel A, Ciancanelli M, Meyts I, Maniatis T, Soumelis V, Amara A, Nussenzweig M, Garcia-
702 Sastre A, Krammer F, Pujol A, Duffy D, Lifton R, Zhang SY, Gorochov G, Beziat V, Jouanguy
703 E, Sancho-Shimizu V, Rice CM, Abel L, Notarangelo LD, Cobat A, Su HC, Casanova JL. 2020.
704 Inborn errors of type I IFN immunity in patients with life-threatening COVID-19. Science
705 https://doi.org/10.1126/science.abd4570.

706 30. Daffis S, Samuel MA, Keller BC, Gale M Jr, Diamond MS. 2007. Cell-specific IRF-3
707 responses protect against West Nile virus infection by interferon-dependent and -
708 independent mechanisms. PLoS Pathog 3:e106.

709 31. Menachery VD, Leib DA. 2009. Control of Herpes Simplex Virus Replication Is Mediated
710 through an Interferon Regulatory Factor 3-Dependent Pathway. J Virol 83:12399–12406.

711 32. Honda K, Yanai H, Negishi H, Asagiri M, Sato M, Mizutani T, Shimada N, Ohba Y, Takaoka
712 A, Yoshida N, Taniguchi T. 2005. IRF-7 is the master regulator of type-I interferon-
713 dependent immune responses. Nature 434:772–7.

714 33. Schilte C, Buckwalter MR, Laird ME, Diamond MS, Schwartz O, Albert ML. 2012. Cutting
715 Edge: Independent Roles for IRF-3 and IRF-7 in Hematopoietic and Nonhematopoietic
716 Cells during Host Response to Chikungunya Infection. JI 188:2967–2971.

717 34. Chen HW, King K, Tu J, Sanchez M, Luster AD, Shresta S. 2013. The roles of IRF-3 and IRF-
718 7 in innate antiviral immunity against dengue virus. J Immunol 191:4194–201.

719 35. Canivet C, Rhéaume C, Lebel M, Piret J, Gosselin J, Boivin G. 2018. Both IRF3 and
720 especially IRF7 play a key role to orchestrate an effective cerebral inflammatory response
721 in a mouse model of herpes simplex virus encephalitis. J Neurovirol 24:761–768.

722 36. Jasperse BA, Mattocks MD, Noll KM, Ferris MT, Heise MT, Lazear HM. 2022.
723 Neuroinvasive flavivirus pathogenesis is restricted by host genetic factors in
724 Collaborative Cross mice, independently of Oas1b. bioRxiv
725 https://doi.org/10.1101/2022.10.24.513634.

726 37. Cartwright HN, Barbeau DJ, Doyle JD, Klein E, Heise MT, Ferris MT, McElroy AK. 2022.
727 Genetic diversity of collaborative cross mice enables identification of novel rift valley
728 fever virus encephalitis model. PLOS Pathogens 18:e1010649.

729 38. Brown AJ, Won JJ, Wolfisberg R, Fahnøe U, Catanzaro N, West A, Moreira FR, Batista MN,
730 Ferris MT, Linnertz CL, Leist SR, Nguyen C, De la Cruz G, Midkiff BR, Xia Y, Montgomery
731 SA, Billerbeck E, Bukh J, Scheel TKH, Rice CM, Sheahan TP. 2023. Host genetic variation
732 guides hepacivirus clearance, chronicity, and liver fibrosis in mice. preprint.
733 Microbiology.

734 39. Sato M, Suemori H, Hata N, Asagiri M, Ogasawara K, Nakao K, Nakaya T, Katsuki M,
735 Noguchi S, Tanaka N, Taniguchi T. 2000. Distinct and essential roles of transcription
736 factors IRF-3 and IRF-7 in response to viruses for IFN-alpha/beta gene induction.
737 Immunity 13:539–48.

738 40. Vaquero-Garcia J, Barrera A, Gazzara MR, González-Vallinas J, Lahens NF, Hogenesch JB,
739 Lynch KW, Barash Y. 2016. A new view of transcriptome complexity and regulation
740 through the lens of local splicing variations. eLife 5:e11752.

41. R Core Team. 2021. R: A Language and Environment for Statistical Computing. https://www.R-project.org/.

42. Venables WN, Ripley BD. 2002. Modern Applied Statistics with S. Fourth EditionFourth. Springer. https://www.stats.ox.ac.uk/pub/MASS4/.

43. Bourdon M, Montagutelli X. 2022. stuart: an R package for the curation of SNP genotypes from experimental crosses. G3 (Bethesda) jkac219.

44. Broman KW, Wu H, Sen S, Churchill GA. 2003. R/qtl: QTL mapping in experimental crosses. Bioinformatics 19:889–890.

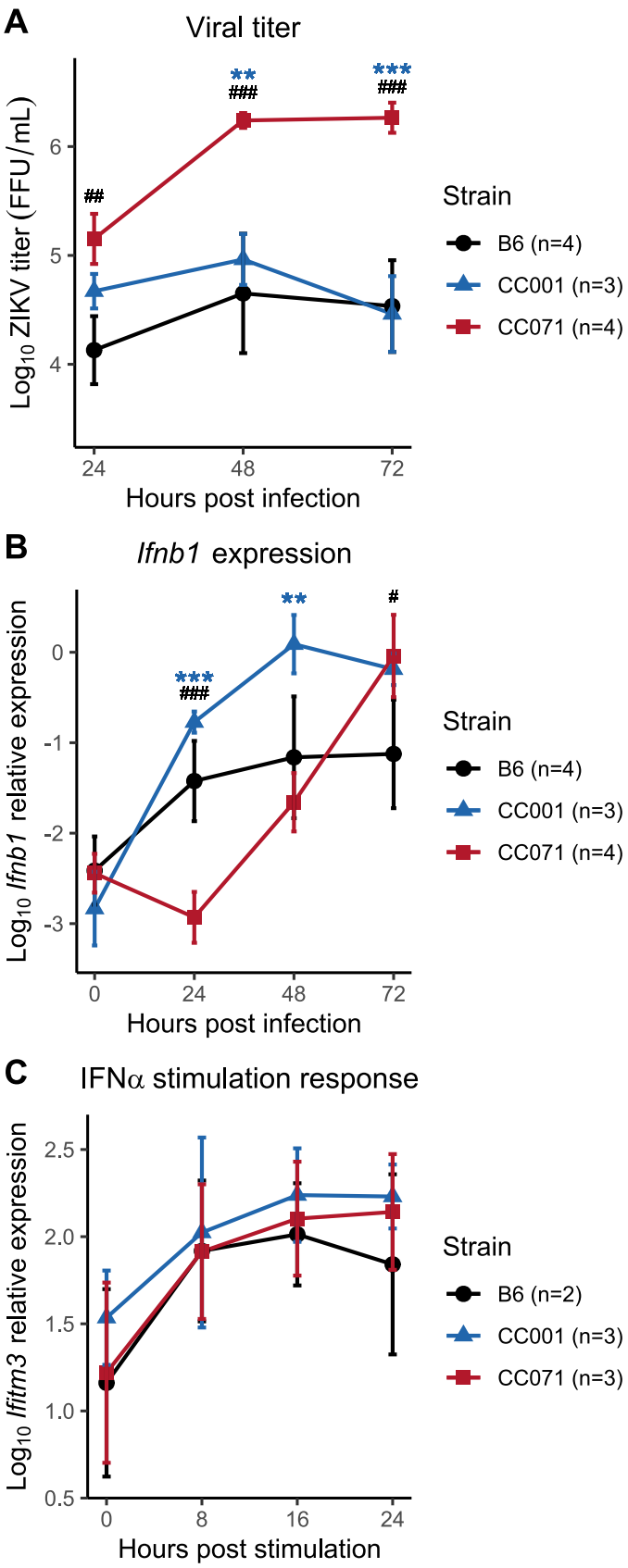

Figure 1. CC071 MEFs fail to control viral replication, with delayed *Ifnb1* expression but normal response to IFN-I. (A,B) MEFs derived from B6 (black circles), CC001 (blue triangles) and CC071 (red squares) were infected with ZIKV at a MOI of 5 and analyzed 24, 48 and 72 h.p.i. (A) Viral titer in supernatants was quantified by FFA. (B) *Ifnb1* expression was normalized to *Tbp* reference gene. Data are mean +/- sem from 3 to 4 biological replicates per strain (MEFs derived from individual embryos). (C) MEFs were stimulated with recombinant IFNα. *Ifitm3* relative expression normalized to *Tbp* reference gene is shown as an example of ISG. Data are mean +/- sem from 2 to 3 biological replicates. Blue asterisks and black hashes show statistical significance of CC071 compared to CC001 and to B6, respectively (ANOVA followed by Tukey HSD, */# $p < 0.05$, **/## $p < 0.01$, *** $p < 0.001$).

A

Comparison of CC strains haplotypes of IFN–I pathway genes

Gene	Protein	CC071	CC001	CC005	CC026	CC021	CC006	CC025	CC039	CC060
Ddx58	RIG–I	HH	BB	EE	CC	HH	AA	HH	AD	EE
Ifih1	LGP2	GG	AA	DD	HH	GG	BB	AA	BB	CC
Dhx58	MDA–5	FF	EE	DD	HH	FF	DD	FF	FF	EE
Tlr3	TLR3	AA	AA	BB	CC	EE	AA	BB	FF	CC
Mavs	MAVS	CC	AA	DD	HH	GG	CC	DD	HH	DD
Ticam1	TRIF	CC	AA	EE	BB	CC	DD	HH	AA	EE
Azi2	NAP1	EE	DD	FF	BB	FF	EE	GG	CC	EE
Traf3	TRAF3	HH	HH	GG	CC	FF	CC	CC	AA	BB
Tbk1	TBK1	HH	DD	GG	HH	AA	FF	AA	GG	BB
Ikbke	IKKε	CC	EE	CC	AA	EE	CC	CC	GH	AA
Irf3	IRF3	FF	FF	HH	BB	CC	DD	EE	HH	BB
Irf7	IRF7	HH	BB	DD	DD	HH	EE	DD	HH	DD
Ifnb1	IFNβ	HH	EE	DD	CC	HH	BB	HH	CC	DE

B

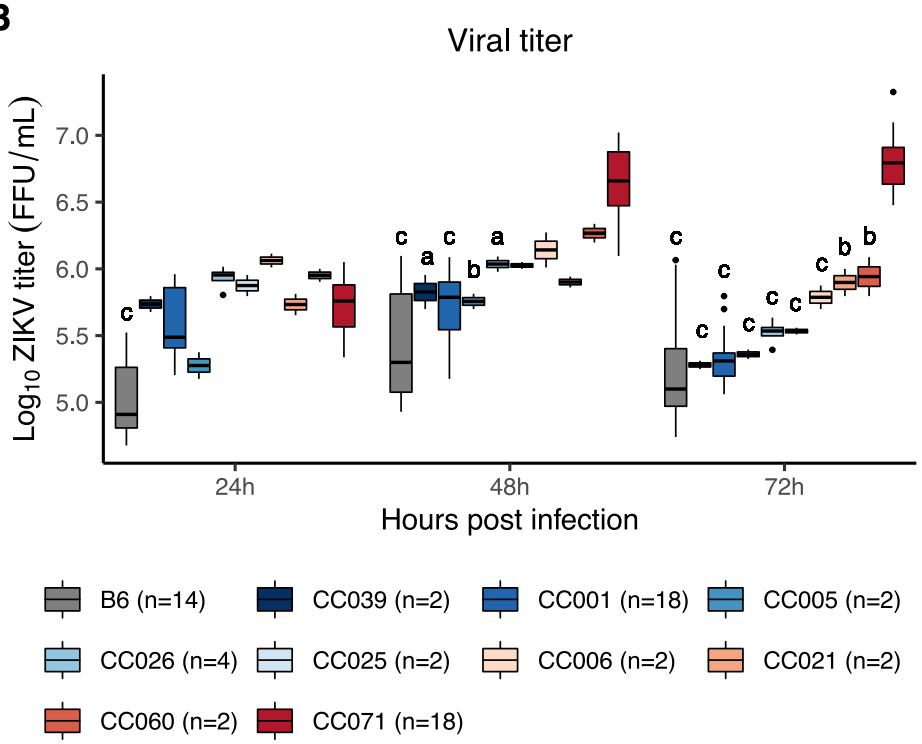

Figure 2. Haplotype analysis fails to identify a genes from the IFN-I induction pathway associated with uncontrolled viral replication. (A) Identification of CC strains which carry the same ancestral haplotype as CC071 at the genes involved in the pathway leading to IFN-I expression. Colored boxes indicate matched haplotypes between CC071 and other CC strains. Letters and colors designate the eight CC founder strains. A: A/J (yellow); B: C57BL/6J; C: 129S1/SvImJ (pink); D: NOD/ShiLtJ; E: NZO/HILtJ (light blue); F: CAST/EiJ (green); G: PWK/PhJ (red); H: WSB/EiJ (purple). Doubled letters (eg AA) indicate homozygous genotypes. Heterozygous genotypes are indicated by the two corresponding letters (eg AD). (B) Kinetics of viral titer in MEFs from CC071 and the 8 CC strains shown in (A). Experimental conditions were as in Figure 1A-C. n: number of technical replicates for each strain. Data are mean +/- sem from the technicalreplicates. Letters show statistical significance between CC071 and other strains. (ANOVA followed by Tukey HSD, a: $p < 0.05$, b: $p < 0.01$, c: $p < 0.001$).

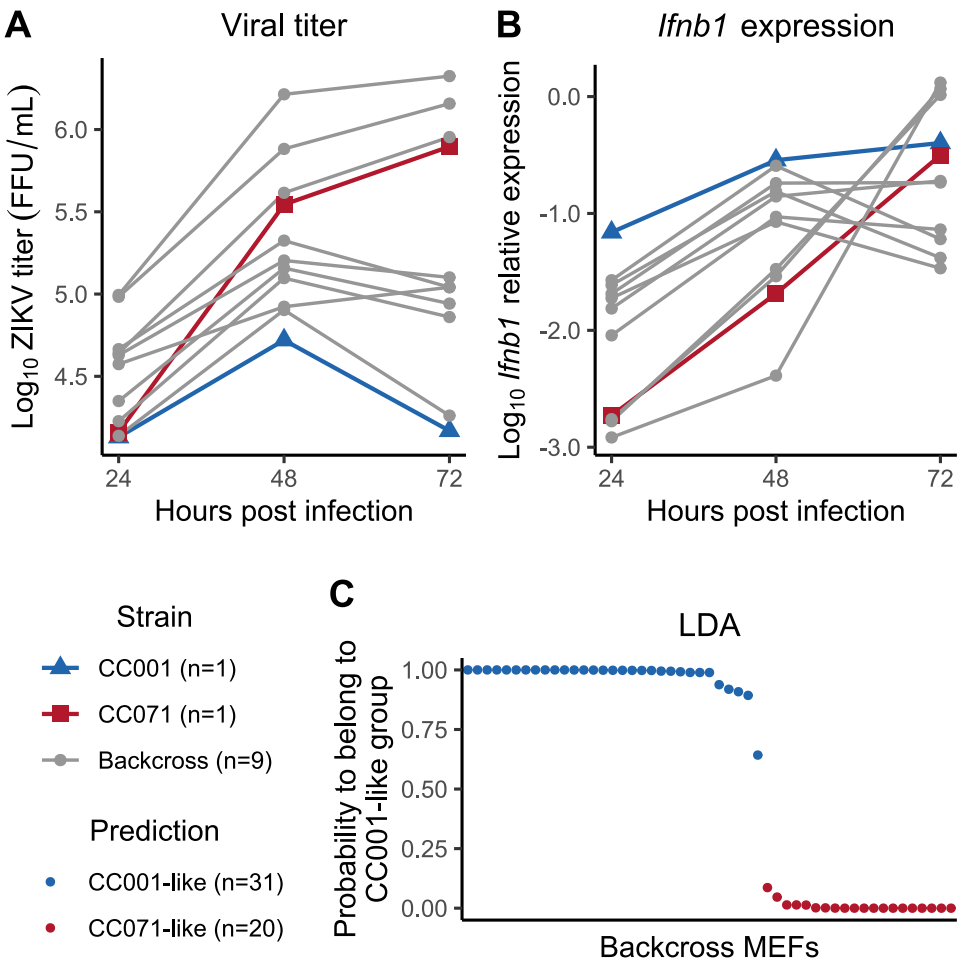

Figure 3. Backcross MEFs display either a CC001-like or a CC071-like phenotype. MEFs derived from CC001 (blue triangles), CC071 (red squares) and backcross (gray circles) embryos were infected with ZIKV at a MOI of 5. (A) Viral titer and (B) Ifnb1 expression in ZIKV-infected MEFs from 9 backcross embryos. Experimental conditions were as in Figure 1A-B. Red and blue curves show the results for CC071 and CC001 MEFs, respectively, from the same infection experiment. (C) Results of LDA on the backcross MEFs. LDA coefficients were calculated from Ifnb1 expression data in CC001 and CC071 infected MEFs and applied to backcross MEFs. The graph shows the probability of each BC MEF to belong to the "CC001-like" group, resulting in two distinct populations shown in blue ("CC001-like") and in red ("CC071-like"). n: number of BC MEFs assigned to each group.

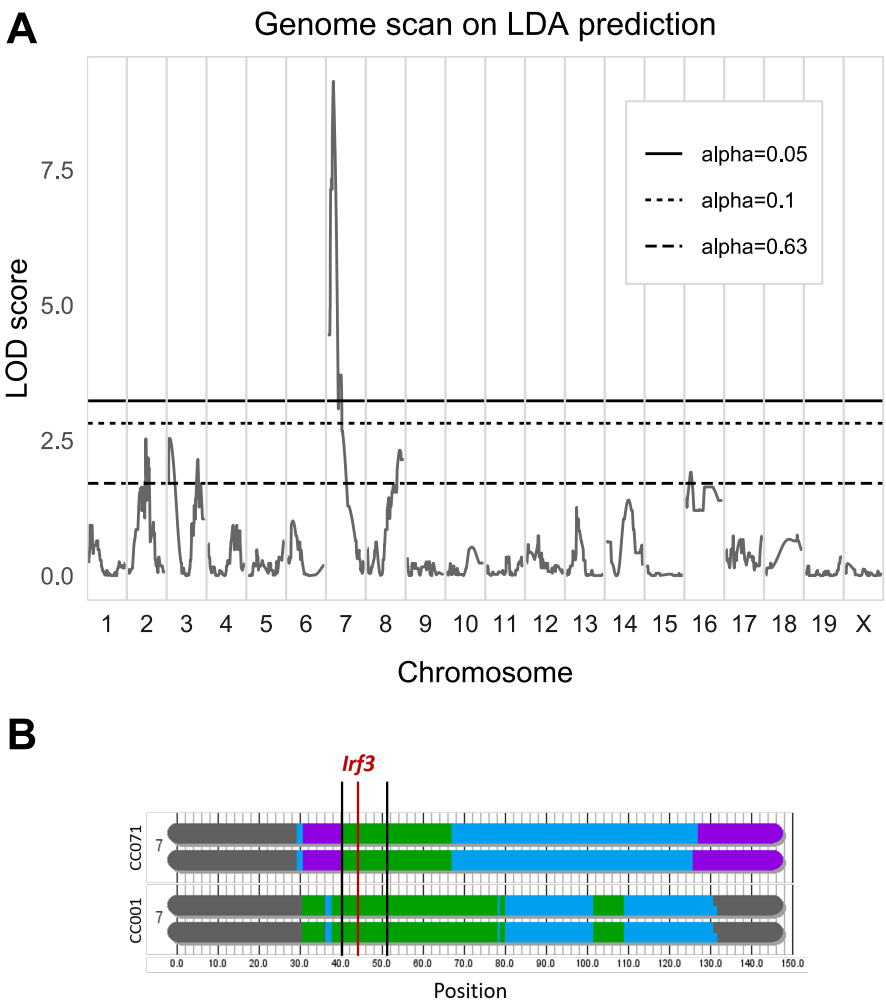

Figure 4. Genetic analysis of *Ifnb1* expression in backcross MEFs identifies a major determinant mapping to the *Irf3* locus. (A) Genome-wide linkage analysis of the LDA classification of backcross MEFs performed with R/qtl. X-axis: genomic location. Y-axis: LOD score of the phenotype-genotype association. Genome-wide significance thresholds (P = 0.05, P = 0.1 and P = 0.63) were computed from 1000 data permutation. The chromosome 7 peak has a LOD score of 9.138. (B) Schematic representation of CC001 and CC071 chromosome 7 haplotypes, from https://csbio.unc.edu/CCstatus/CCGenomes/. Colors represent the CC ancestral haplotypes (same colors as in Figure 2A). Thick vertical black lines show the peak's 95% Bayesian confidence interval (25.9-31.3 cM, corresponding to 40.1-50.6 Mb). The red line shows the position of *Irf3* gene.

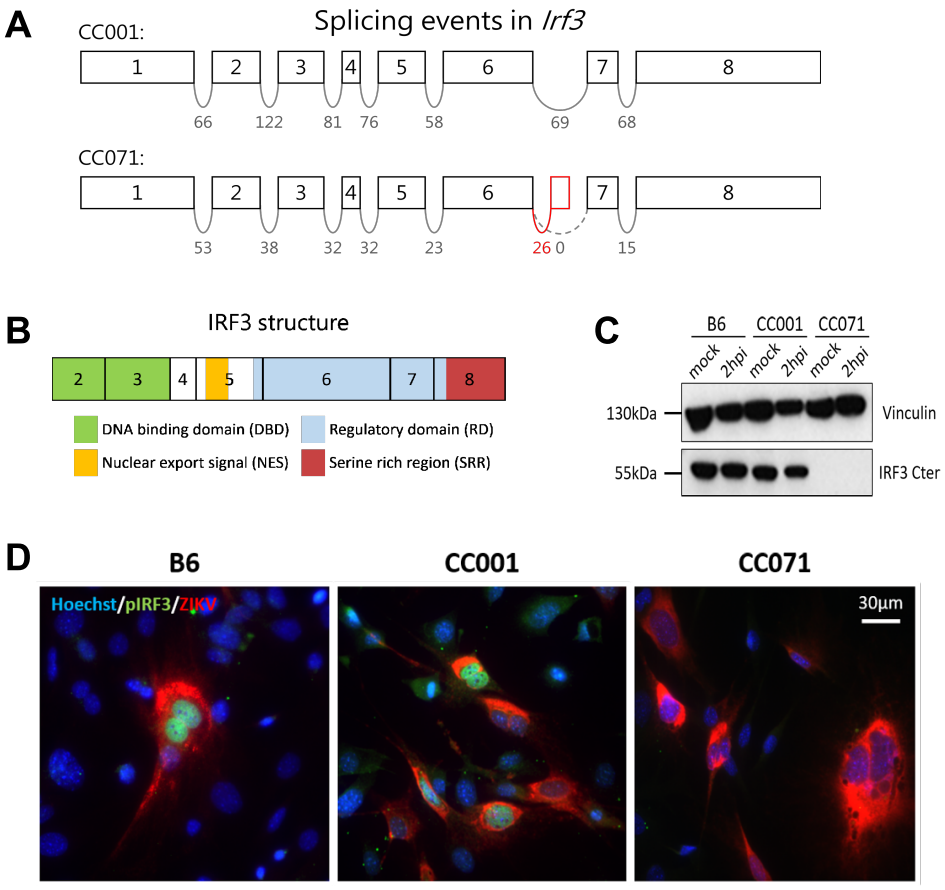

Count	B6	CC001	CC071
Infected cells	24	91	76
pIRF3 positive cells	5	28	0
Percentage	21%	31%	0%

Figure 5. CC071 *Irf3* mRNAs show abnormal splicing, resulting in defective IRF3 protein. Schematic representation of the exons of the *Irf3* gene with the number of reads spanning successive exons in the CC001 and CC071 RNAseq data (one sample of each strain). The red box between CC071's exons 6 and 7 depicts a novel exon resulting from abnormal splicing. (B) Schematic representation of the IRF3 protein structural domains (exon 1 is untranslated). Exon 8 encodes the serine rich region containing the phosphorylation sites for IRF3 activation. (C) Western blot using an anti-C-terminal IRF3 antibody from mock-infected and ZIKV-infected B6, CC001 and CC071 MEFs at 2 h.p.i., showing the absence of full-length IRF3 in CC071 MEFs. Vinculin was used as a loading control. (D) Immunofluorescence using an anti-phosphorylated IRF3 (pIRF3, green) in ZIKV-infected B6, CC001 and CC071 MEFs at 24 h.p.i., showing the absence of pIRF3 in the nucleus of CC071 MEFs upon infection. Red-labeled 4G2 antibody labels ZIKV-infected cells. Cell nuclear DNA labeled by Hoechst (blue). Quantification of the number of infected and pIRF3 positive cells is presented in the table. Proportions were established on 420, 428 and 551 cells for CC001, CC071 and B6, respectively.

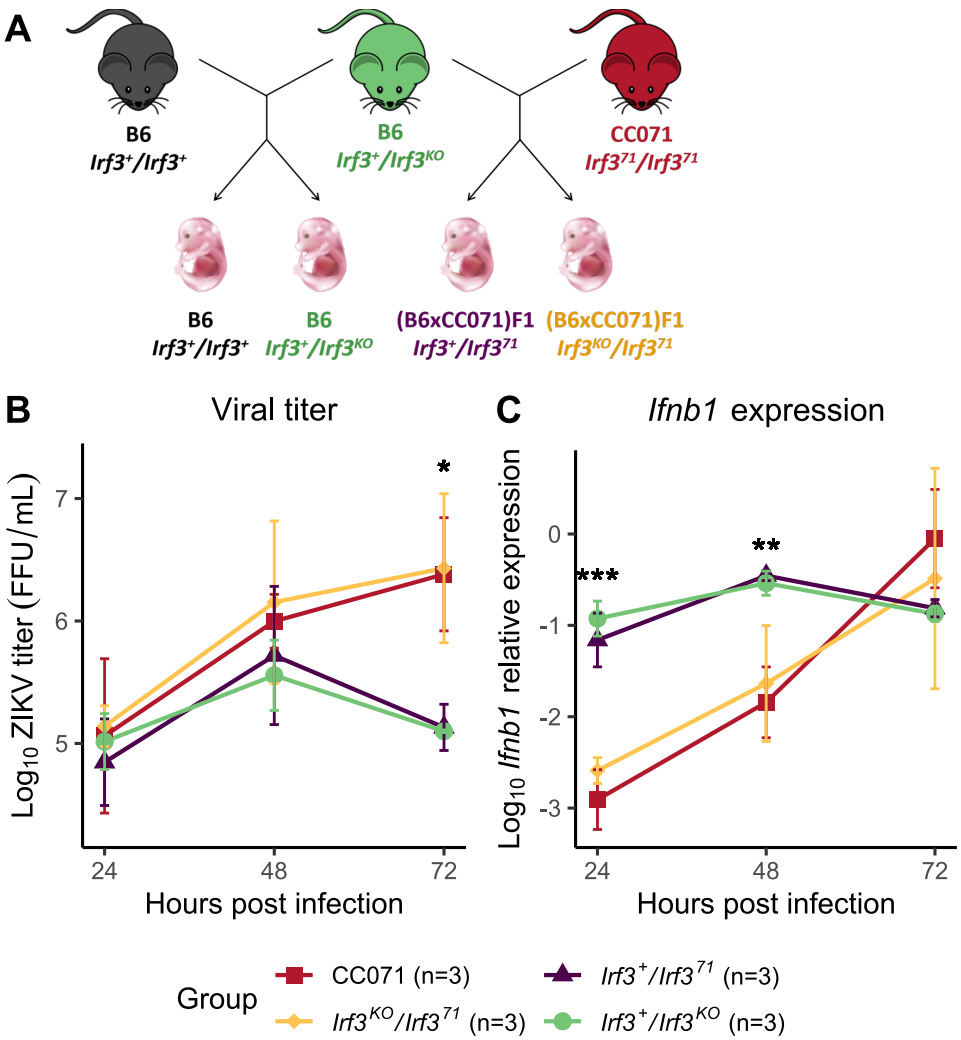

Figure 6. Quantitative complementation test confirms that *Irf3* LOF in CC071 is responsible for uncontrolled viral replication and delayed *Ifnb1* expression. (A) Mice heterozygous for an inactivated *Irf3* allele (B6-$Irf3^{+}/Irf3^{KO}$) were mated with B6 and with CC071 mice to produce four types of embryos from which MEFs were derived. The genetic background and *Irf3* genotype is shown below each type of embryos. (B) Viral titer and (C) *Ifnb1* expression in ZIKV-infected MEFs. Experimental conditions were as in Figure 1A-B. Data are mean +/- sem from 3 biological replicates for each group. At every time point, the comparison of either CC071 or $Irf3^{KO}/Irf3^{71}$ with either $Irf3^{+}/Irf3^{71}$ or $Irf3^{+}/Irf3^{KO}$ gave identical statistical significance (ANOVA followed by post-hoc Tukey HSD, * $p < 0.05$, ** $p < 0.01$, *** $p < 0.001$).

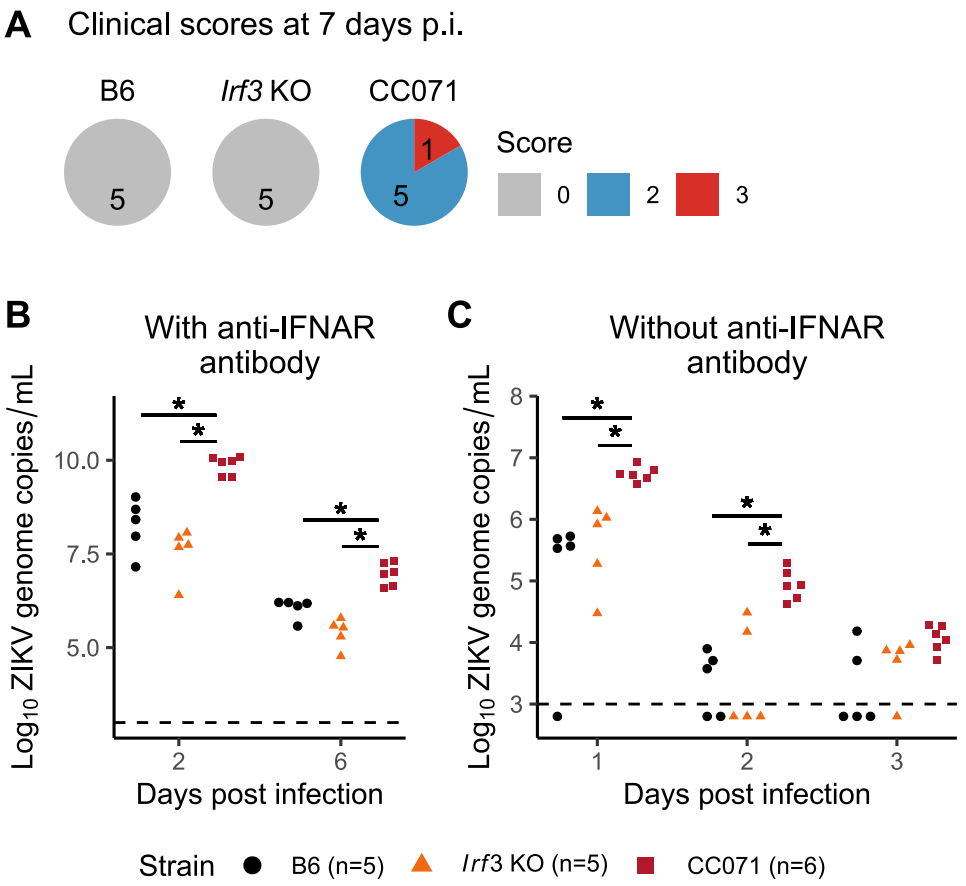

Figure 7. *Irf3* LOF is not sufficient to explain CC071 susceptibility to ZIKV infection *in vivo*. CC071, B6-$Irf3^{KO}$ and B6 mice were infected IP with 10^7 FFUs of ZIKV and monitored for 7 days, with (A,B) or without (C) IP injection of 2 mg of MAR1-5A3 IFNAR-blocking monoclonal antibody 24 h before infection. (A) Average clinical score of anti-IFNAR-treated at day 6 p.i. (B,C) Plasma viral load measured by RT-qPCR. Each dot represents one mouse. Groups were compared by Kruskal-Wallis test followed by Wilcoxon test with Bonferroni correction for multiple testing (* $p < 0.05$).

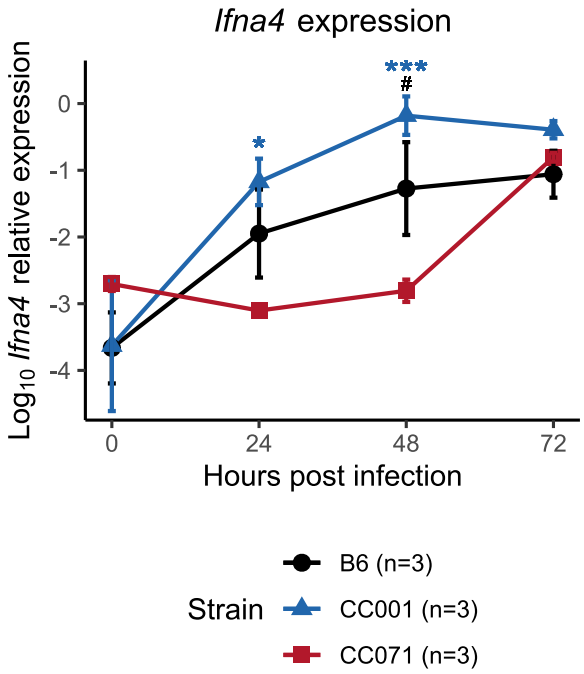

Figure S1. *Ifna4* expression is delayed in ZIKV-infected CC071 MEFs. MEFs derived from B6 (gray circles), CC001 (blue triangles) and CC071 (red squares) were infected with ZIKV at a MOI of 5. *Ifna4* expression was determined by RT-qPCR on MEFs total RNA by normalizing to *Tbp* housekeeping gene. Data are mean +/- sem from 3 biological replicates. One CC001, one B6 and one CC071 replicates at 0 hpi and one CC071 replicate at 24 hpi were below the limit of detection. Blue asterisks and black hashes show statistical significance of CC071 compared to CC001 and to B6, respectively (ANOVA followed by post-hoc Tukey HSD, */# $p < 0.05$, *** $p < 0.001$).

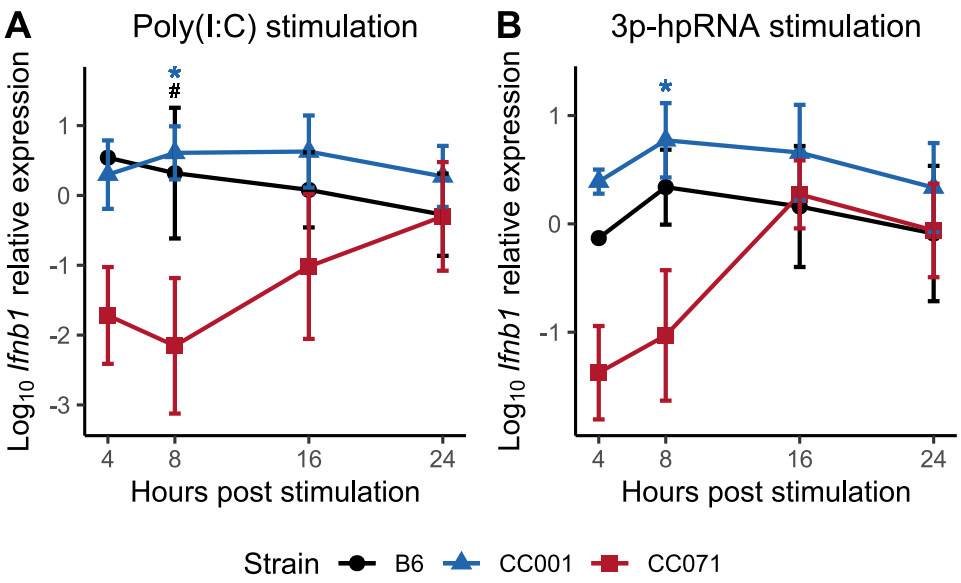

Figure S2. Delayed IFN-I expression in CC071 MEFs results from a constitutive defect in innate antiviral response. MEFs were transfected with either (A) poly(I:C), which activates both TLR and RIG-I pathways, or (B) 3p-hpRNA, a RIG-I agonist. *Ifnb1* expression was determined as in Figure 1B. Data are mean +/- sem from 3 biological replicates for CC001 and CC071 (2 at 4 hours) or 2 biological replicates for B6 (1 at 4 hours). Blue asterisks and black hashes show statistical significance of CC071 compared to CC001 and to B6, respectively (ANOVA followed by post-hoc Tukey HSD, */# $p < 0.05$).

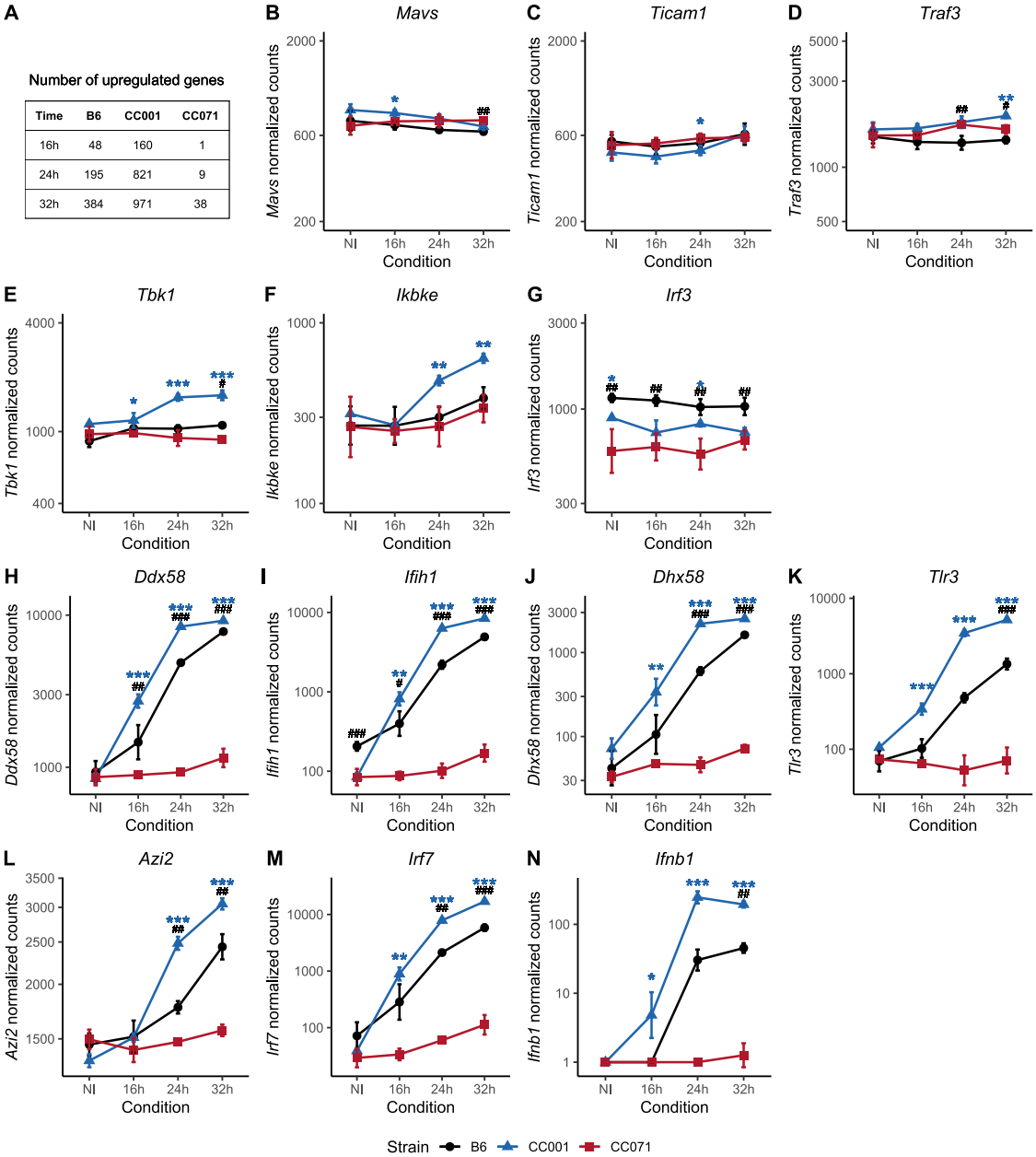

Figure S3. Expression of genes involved in the *Ifnb1* induction pathway in ZIKV-infected MEFs of B6, CC001 and CC071 strains. MEFs derived from B6 (black circles), CC001 (blue triangles) and CC071 (red squares) were infected with ZIKV at a MOI of 5. mRNA expression levels were measured by RNAseq in non-infected (NI) and ZIKV-infected MEFs. (A) Number of upregulated genes per strain at 16, 24 and 32 hpi (B-G) Genes constitutively expressed. (H-N) Genes which expression is induced by the IFN-I response (ISGs). Expression levels are shown on a logarithmic scale. For *Ifnb1* expression, null counts were transformed to 1. Data are mean +/- sem from 3 biological replicates. Blue asterisks and black hashes show statistical significance of CC071 compared to CC001 to B6, respectively (ANOVA followed by post-hoc Tukey HSD, */# $p < 0.05$, **/## $p < 0.01$, ***/### $p < 0.001$).

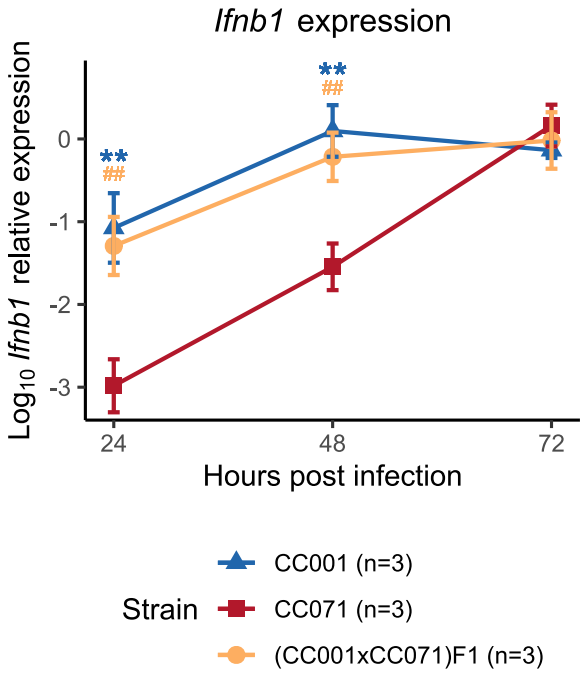

Figure S4. (CC001xCC071)F1 MEFs show normal induction of *Ifnb1*. *Ifnb1* expression upon ZIKV infection in CC001, CC071 and (CC001xCC071)F1 MEFs determined as in Figure 1B. Data are mean +/- sem from 3 biological replicates. Blue asterisks and orange hashes show statistical significance of CC071 compared to CC001 and to F1, respectively (ANOVA followed by post-hoc Tukey HSD, **/## $p < 0.01$).

Supplementary methods

MEFs stimulation with poly(I :C) and 3p-hpRNA

For intracellular stimulation with Poly(I:C) or with 3p-hpRNA, MEFs were seeded at 1.10^5 cells per well in 12-well plates the day before stimulation, transfected with 1 µg/mL Poly(I:C) (InvivoGen Cat#vac-pic) or 0.5 µg/mL 3p-hpRNA (InvivoGen Cat#tlrl-hprna) using 5 µL Lipofectamine LTX and 1 µL for poly(I:C) stimulation or 0.5 µL for 3p-hpRNA stimulation of Plus Reagent (ThermoFischer Scientific Cat#15338100), according to the manufacturer's instructions. After stimulation, MEFs were incubated for 8 to 24 hours.

RNA sequencing

MEF RNA was prepared as described in the main text. RNA integrity and quantification were assessed using the RNA Nano 6000 Assay Kit of the Bioanalyzer 2100 system (Agilent Technologies, CA, USA). One microgram of high-quality RNA samples (RIN > 9.2) representing biological triplicates were submitted to Novogene for RNA-sequencing (Novogene Beijing, China). Poly-A selected RNA was used for paired-end library preparation and transcriptome sequencing. Sequencing libraries were generated using NEBNext® UltraTM RNA Library Prep Kit for Illumina® (NEB, USA) following manufacturer's instructions. The library preparations were sequenced on an Illumina platform and paired-end reads were generated. The RNA-seq analysis was performed with Sequana 0.9.8 (1). In particular, we used the RNA-seq pipeline https://github.com/sequana/sequana_rnaseq) built on top of Snakemake 6.1.1 (2). Briefly, reads were trimmed from adapters using Cutadapt 2.7 then mapped to the Mus musculus genome assembly GCA_000001635.8 from NCBI using STAR 2.7.3a (3). FeatureCounts 1.6.4 (4) was used to produce the count matrix, assigning reads to features using corresponding annotation v92 from NCBI with strand-specificity information. Quality control statistics were summarized using MultiQC 1.6 (5). Clustering of transcriptomic profiles were controlled using a Principal Component Analysis (PCA). Differential expression testing was conducted using DESeq2 library 1.24.0 (6) scripts indicating the significance (Benjamini-Hochberg adjusted p-values, false discovery rate FDR < 0.05) and the effect size (fold-change) for each comparison.

1. Cokelaer T, Desvillechabrol D, Legendre R, Cardon M. 2017. “Sequana”: a Set of Snakemake NGS pipelines. JOSS 2:352.

2. Köster J, Rahmann S. 2012. Snakemake—a scalable bioinformatics workflow engine. Bioinformatics 28:2520–2522.

3. Dobin A, Davis CA, Schlesinger F, Drenkow J, Zaleski C, Jha S, Batut P, Chaisson M, Gingeras TR. 2013. STAR: ultrafast universal RNA-seq aligner. Bioinformatics 29:15–21.

4. Liao Y, Smyth GK, Shi W. 2014. featureCounts: an efficient general purpose program for assigning sequence reads to genomic features. Bioinformatics 30:923–930.

5. Ewels P, Magnusson M, Lundin S, Käller M. 2016. MultiQC: summarize analysis results for multiple tools and samples in a single report. Bioinformatics 32:3047–3048.

6. Love MI, Huber W, Anders S. 2014. Moderated estimation of fold change and dispersion for RNA-seq data with DESeq2. Genome Biol 15:550.

TabS1

Gene	Forward	Reverse
Ifnb1	CAGCTCCAAGAAAGGACGAAC	GGCAGTGTAACTCTTCTGCAT
Ifnα4	TGATGAGCTACTACTGGTCAGC	GATCTCTTAGCACAAGGATGGC
ZIKA *Env*	CCGCTGCCCAACACAAG	CCACTAACGTTCTTTTGCAGACAT
Ifitm3	ACTGTGATCAACATGCCCAGAG	CTTCCGATCCCTAGACTTCACG
Tbp	AGAACAATCCAGACTAGCAGC	GGGAACTTCACATCACAGCTC

TabS2

Immunofluorescence antibodies

Primary/secondary	Antibody	Species	Dilution	Reference
Primary	ZIKV envelop protein	Mouse	1:200	4G2 antibody from ATCC hybridoma
Primary	Phosphorylated IRF3	Rabbit	1:250	Cell Signaling Technology Cat#29047
Secondary	Anti-rabbit AlexaFluor-488-conjugated IgG	Goat	1:500	Invitrogen Cat#A-11034
Secondary	Anti-mouse AlexaFluor-594-conjugated IgG	Donkey	1:500	Invitrogen Cat#A-21203

Western blot antibodies

Primary/secondary	Antibody	Species	Dilution	Reference
Primary	IRF3 Cter	Rabbit	1:1000	Cell Signaling Cat#4302
Primary	Vinculin	Rabbit	1:1000	Proteintech Cat# 26520-1-AP
Secondary	Rabbit IgG HRP Linked Whole Ab	Donkey	1:10,000	Sigma Cat# GENA934-100UL